Decay of nuclear magnetization by diffusion in a parabolic magnetic field: An exactly solvable model

Pierre Le Doussal*
Institute for Advanced Study, Princeton, New Jersey 08540

Pabitra N. Sen
Schlumberger-Doll Research, Old Quarry Road, Ridgefield, Connecticut 06877-4108
(Received 4 December 1991)

An exact expression for the decay of the transverse magnetization of spins diffusing in a field $(B_0+g_1z+g_2z^2)\hat{\mathbf{z}}$ reveals that a natural length scale $l_c=(8D/\gamma g_2)^{1/4}$, and a frequency associated with it $\Omega_0=4D/l_c^2$ govern the problem. Here D is the diffusion constant and γ is the gyromagnetic ratio. l_c is the size of the packet of magnetization at long times, i.e., $\Omega_0 t \gg 1$. For porous media we estimate $l_c \sim (R_p l^*)^{1/2}$ where R_p is the pore size and $l^{*2}=D/\Delta\omega$, where $\Delta\omega$ is the spread in Larmor frequency (inhomogeneous broadening). For typical experimental conditions, $l^* \sim 3$ μm; therefore in rocks the effects of the extrema of the magnetic field can be as important as the wall effects. To estimate finite-pore-size effects we localize the spins in a potential well of size R_p. We find that the effective pore size is l_c or R_p, whichever is smaller. At short times, the magnetization density $|M(z,t)| \sim \exp[-D\gamma^2(g_1+2g_2z)^2t^3/3]$, i.e., it is permissible to use an effective local gradient. The magnetization decays rapidly where the magnetic field varies rapidly—thus the magnetization accumulates at the extremum of the field. At long times, the magnetization decays as $\exp(-\Omega_0 t/2)$, as opposed to $\exp(-t^3)$, in a uniform gradient. The phase distribution is not Gaussian, which leads the decay rate $\Omega_0 \sim \sqrt{g_2}$ to be a nonanalytic function of g_2. There is an overall shift $\Omega_0/2$ (the "g-shift") in the effective Larmor frequency, due to diffusion. The signal from a pulse-field-gradient experiment is similar to that of an isolated pore of size l_c. We compute the Hahn- and Carr-Purcell-Meiboom-Gill-(CPMG-) echo envelopes and find qualitative agreement with experimental data on porous media. Extracting g_2 from the observed inhomogeneous broadening gives correct crossover times toward the linear regime. The slopes of the CPMG envelopes depend linearly on pulse spacing, as observed experimentally.

I. INTRODUCTION

Recently, there has been a vigorous interest in using NMR techniques[1] to obtain information about the microgeometry of porous media. Pore sizes, their connectivity, and tortuosity control fluid flow and other transport processes that are important in permeation in rocks (in the oil industry, hydrogeology, and in the confinement of wastes), heterogeneous catalysis, biological perfusion, and numerous other phenomena in porous systems.

Much effort has gone into using the longitudinal-relaxation-rate $1/T_1$ and transverse-relaxation-rate $1/T_2$ data to infer pore-size distribution in rocks. The rates are enhanced by the paramagnetic impurities that are present on the pore walls and therefore the decay rates depend on surface area and pore geometry.[2-4] But a major difficulty in interpreting T_2 data is the additional decay due to internal field inhomogeneities.

The pulsed-field-gradient spin-echo (PFGSE) technique has been used for many years now[5-8] to characterize diffusion and flow in such systems. In these experiments the gradient pulse plays the role of a wave vector probing the structure of the obstacles to the diffusion. Callaghan *et al.*[8] have pointed out that the PFGSE technique is particularly promising because it can provide spatial information at a resolution (submicrometer) which is higher than that achievable with conventional NMR imaging (NMRI), which is also used extensively in porous media.

Application of NMRI to study fluid distribution and fluid flow in porous rocks has become very active.[9] The position of the pore fluid is inferred from the local magnetic field, which is controlled via an externally applied field gradient, whose direction can be changed. Both proton densities and T_2 images have been studied.[9] Finally, using high magnetic fields, chemical shift has been used to distinguish between water and oil in a pore space.[9]

The main obstacle in fully exploiting PFGSE, NMRI, and T_2 data (usually derived by sophisticated spin-echo techniques[10]) is the influence of internal field inhomogeneities. When a porous medium, such as sandstone, is placed in a homogeneous magnetic field, the internal local magnetic field is generally inhomogeneous, i.e., varies from point to point. This arises due to a difference between the magnetic susceptibility of the grain and that of the pore fluid.[3,9,11-13] Obviously, any inhomogeneity would alter the local field and hence affect the spatial resolution in NMRI, especially in sandstones, which often contain enough paramagnetic impurities to make the problem worse. Also, any discrimination between oil and water due to the intrinsic difference in chemical shift might be masked by local field inhomogeneity. For ex-

ample, the local field at a given location may exactly cancel the expected chemical shift and oil may be indistinguishable from water.

In addition to the internal field inhomogeneities, there are inhomogeneities of the applied field. In Ref. 11, it has been emphasized that the coils which are used to produce the external field gradients actually give uniform gradients only near their center. Thus, much of the sample volume could be exposed to a nonuniform gradient, especially when the coils are placed close to the sample, as often is done to create large field gradients.

At present, there is no complete and exact theory for treating diffusion effects in a general nonuniform gradient. The purpose of this paper is to present a simple, exactly solvable model of an inhomogeneous field in which the gradient itself varies linearly, i.e., a parabolic field. Although the choice of a parabolic field as the first step beyond the uniform gradient is natural, not until very recently was such a field produced and studied in the laboratory by Bendel.[14] Also, an apparatus[15] intended to be used in oil fields actually produces parabolic fields. In both cases, the parabolic field is externally imposed rather than originating from the local inhomogeneities. Often, such tools are calibrated by immersing them in a large tank of water.

Recently, however Mitra and Le Doussal[16] have obtained a general framework for treating random fields exactly based on a connection with critical phenomena. Although the decay of the magnetization at very long time (e.g., diffusion over many pores) was obtained exactly using universality, the intermediate-time behavior, which is of most interest for experiments on rocks, where the decay is fast, is more difficult to compute in this framework. We consider the simple model studied here as a first step toward understanding intermediate-time behavior in more complex inhomogeneous fields. This model is also useful to assess the validity of various approximate models, for example, those based on the Gaussian-phase approximation. Finally we think that the parabolic field is a good model for developing intuition for porous media, where the field landscape can be pictured as a collection of hills and valleys (parabolas and saddle points) of typical pore size (Fig. 1).

In the absence of a usable theory of inhomogeneous

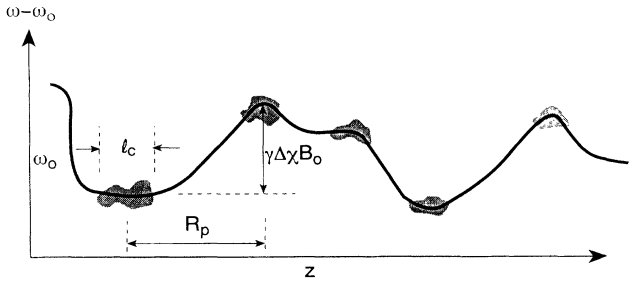

FIG. 1. A schematic diagram showing a possible terrain of local magnetic field, in a pore of a random medium, as a function of distance. Dots are to show the accumulation of magnetization at the extrema.

gradients, the usual practice has been to replace the inhomogeneities by some effective fictitious uniform field gradient. This is only an approximation, since, clearly the local fields are more inhomogeneous than is suggested by a constant gradient. Ingenious pulse sequences have been proposed[10] to minimize the effects of this effective uniform background field gradient for PFGSE in infinite systems. Similarly, for T_2, the usual practice[3,12,13,17] is to use the following formula,[18,19] which strictly speaking is valid only for free diffusion in a uniform unbounded gradient $B_z = B_0 + g_1 z$:

$$M(t) = e^{-1/3 D\gamma^2 g_1^2 t^3 - t/T_{2B}} . \tag{1.1}$$

Here D is the diffusion constant, γ is the gyromagnetic ratio, and T_{2B} the bulk decay constant. Several algorithms have been used for estimating this effective uniform gradient. For example, Glasel and Lee[12] propose the use of the average gradient and Majumdar and Gore[13] propose the use of the variance of the (random) field gradient. There is now much evidence that this approach is not satisfactory. Kenyon[17] noted that the transverse-magnetization decay observed during a Carr-Purcell[18] spin-echo measurement could not be represented by the theories of unbounded diffusion in a constant locally generated field gradient. Kleinberg and Horsfield[3] observed that even when the influence of pore walls was included [using the Gaussian approximation,[20] and an ansatz for spin echoes, see Sec. V C (iii)], the uniform-magnetic-gradient approximation to the local field was too crude to explain their rock data quantitatively.[3]

On the other hand, Bendel[14] experimentally produced a parabolic field and observed that the decay rate deviated from the t^3 dependence for the Hahn echo in the bulk water. Unfortunately, he shows data only for early times (signal decayed only to one fifth of its initial value) where the nontrivial effects beyond an effective-local-gradient approximation have not shown up. He found that the uniform-gradient result, Eq. (1.1), with the gradient replaced by $2g_2 z$, and integrating the amplitude, Eq. (1.1), over the sample volume gave a reasonable answer for the early times he considered. We show below that his model would fail at longer times and we suggest that experiments should be extended to longer times. The departure from the average-gradient theory is manifest in his experiments on water in the pores of a sand exposed to a large external field (200 MHz). This latter system has extremely large pores and the wall effects are presumably small. In this case his model failed both for the Hahn echoes and the Carr-Purcell echoes. The data have features similar to those observed by Kenyon,[17] i.e., faster than exponential decay at early times but exponential decay at late times. The slopes of different decay curves for different pulse spacing t_1 do not scale as t_1^2, which is the result for a uniform gradient. We show below that we can explain his data at all times using the exact solution for a parabolic field. We show elsewhere that for sphere packing the interstitial field is reasonably well approximated by a parabolic field.

Most of the attempts to describe inhomogeneous fields and wall effects beyond the effective-uniform-gradient ap-

proximation have used yet another approximation, the Gaussian-phase approximation. Tarczon and Halperin,[11] for instance, have given a calculation for the influence of an arbitrary inhomogeneous field but assume that the distribution of the total dephasing $\phi(t)=\int_0^t d\tau\,\omega(r(\tau))$ accumulated by a single diffusing spin is exactly Gaussian [$\omega(r)$ is the local Larmor frequency]. This is also called second-cumulant approximation, and the magnetization decay is set equal to

$$\exp\{-\tfrac{1}{2}[\langle\phi(t)^2\rangle-\langle\phi(t)\rangle^2]\}\ , \tag{1.2}$$

where $\langle\cdots\rangle$ denotes an average over all random walks. Equation (1.2) is the first term of a systematic expansion in higher cumulants. Although this approximation holds for short times, and is exact for all times for a uniform gradient in an unbounded medium, it was shown in Ref. 16 that for random fields the cumulant expansion usually breaks down and that in three dimensions large corrections arise for larger time, or stronger disorder. In low dimensions ($d=1,2$) the Gaussian approximation is totally incorrect. For example, the second-cumulant analysis would predict a long-time free-induction decay in one dimension $\exp(-ct^{3/2})$ rather than the correct exponential decay.[16] Here also we find that for the simple models we consider, the distribution of phases is not Gaussian, even in the absence of a wall. The walls[21] also cause a deviation from a Gaussian distribution. The much-used calculation of Neuman[20] for finite-size pores is at best an approximation, and in particular the claim that the distribution of phases tends to be Gaussian at long times is incorrect.[22]

To summarize the above discussion, internal field inhomogeneities cause major problems with NMRI, T_2, and PFGSE techniques and no exact theories of nonuniform fields exist. In this paper we work out an exactly solvable model as a first step.

The main results of the paper are as follows: We find that for diffusion in the unbounded parabolic field $(B_0+g_1z+g_2z^2)\hat{\mathbf{z}}$ there is a natural length scale $l_c=(8D/\gamma g_2)^{1/4}$. This turns out to be the size of the packet of magnetization at long times, i.e., $\Omega_0 t\gg 1$, where $\Omega_0=4D/l_c^2$ is related to the inverse time of diffusion over the distance l_c. Using a simple estimate for g_2, we find that $l_c\sim(R_p l^*)^{1/2}$ where R_p is the pore size and l^* corresponds to a diffusion distance over the time interval given by the inverse of the spread in Larmor frequency arising from the field inhomogeneities. For typical experimental conditions, l^* is ~ 3 μm. In rocks the pore size is also of this order, therefore, the effects of the extrema of the magnetic field can be as important as the wall effects. At short times, it is permissible to use an effective local gradient, and the magnetization decays rapidly as $\exp(-t^3)$ where the magnetic field has a rapid spatial variation. The magnetization creeps towards these extrema of the field. This property suggests that an externally applied parabolic field may be used as a local probe. By altering the location of its extremum in the sample, one may probe the magnetization from point to point in the sample. At long times, the magnetization decays as $\exp(-\Omega_0 t/2)$. The phase distribution is very different from a Gaussian since we obtain $\Omega_0\sim\sqrt{g_2}$, i.e., a nonanalytic function as opposed to the Gaussian approximation (1.2), which always gives decays quadratic in the field (and its derivatives). There is an overall shift $\Omega_0/2$ (the "g-shift") in the effective Larmor frequency, due to diffusion. To estimate finite-pore-size effects we extend the above model by further localizing the spins in a potential well of size R_p. A change from t^3 to t dependence also happens when the system has a finite size. The signal from a pulse-field-gradient experiment (PFGSE) is similar to that of an isolated pore of size l_c or R_p, whichever is smaller. The Hahn- and Carr-Purcell-Meiboom-Gill- (CPMG)-echo envelopes show qualitative agreement with experimental data on porous media. Extracting g_2 from the observed inhomogeneous broadening gives correct crossover times towards the linear regime. The slopes of the CPMG envelopes depend linearly on pulse spacing, as observed experimentally.

This paper is arranged as follows: In Sec. II, we derive the expression for the diffusion propagator in a parabolic local field in an unbounded medium. The propagator is then used to compute the spin amplitude under various circumstances in the following sections: in Sec. III, we compute T_2 by computing $M(z,t)$. Section IV considers an artificial model, originally used by Stejskal,[5] for bounded diffusion by the use of an artificial attraction to the center. We compute T_2 and the PFGSE signal. In Sec. V we consider line broadening, the Hahn spin echo and the CPMG echoes in this model. Section VI is the conclusion.

II. GENERAL FORMULATION: THE GREEN'S FUNCTION

In this section we derive the expression for the diffusion propagator in a parabolic local field. The propagator can then be used to compute the spin-echo amplitude for any experimental pulse program. We will make the assumption that the inhomogeneities are weak compared to the uniform static field [see below, following Eq. (2.1)]. This should be a good approximation because the internal field inhomogeneities are created by the susceptibility differences, which are typically of the order of 10^{-5} in rocks, and even less in biological systems. In this limit, when one transforms to the rotating frame, only the components of the internal field inhomogeneities that are parallel to the static external field survive. The components transverse to the external field rotate very fast and may be neglected. Thus, we need only consider the local inhomogeneities in Larmor frequency. A slightly refined statement is that since diffusion is slow (adiabatic) the adiabatic theorem implies that the spins (the random walkers) precess around the local z axis, given by the local direction of the field. The local deviations $B_z(\mathbf{r})-B_0$ are assumed to be small compared to (i) the external static field $B_0\hat{\mathbf{z}}$, so the resonance condition is met by the bandwidth of the rf coils and (ii) the field B_1, which is used to tip the spins by $\pi/2$ or π, so that the total field causing the flip lies as close to the x-y plane as possible. Note that these requirements imply that the local $B(\mathbf{r})$

can be made consistent with Maxwell's equations by adding compensating fields orthogonal to the $\hat{\mathbf{z}}$ direction. But these have negligible influence in the rotating frame.

The equations of motion of the transverse magnetization density $M=M_x+iM_y$, in the rotating frame following a $\pi/2$ pulse, obey Bloch's equation as modified, by Torrey,[19] to include diffusion

$$\frac{\partial M(\mathbf{r},t)}{\partial t}=D\nabla^2 M(\mathbf{r},t)+i\gamma(g_1 z+g_2 z^2)M(\mathbf{r},t) \tag{2.1}$$

with $\exp(i\omega_0-1/T_{2B})t$ factored out, and $\omega_0=\gamma B_0$. Here D is the diffusion constant γ is the gyromagnetic ratio, g_1 is the local field gradient and g_2 is proportional to the second derivative of the field, T_{2B} is the bulk decay rate. It is important to note that for convenience we have chosen g_2 positive, real quantities being independent of the sign of g_2. If R_p is the dimension of the system in the z direction, we will assume it to be sufficiently large for the boundary effects to be negligible, yet $g_1 R_p$ and $g_2 R_p^2$ are small compared to B_0 and B_1. For example, in Bendel's experiment,[14] $B_0\sim 200$ MHz and the overall inhomogeneity is only several hundred Hz.

The above equation has a natural length scale, which will turn out to be the size of the packet of magnetization at long times,

$$l_c=\left[\frac{8D}{\gamma g_2}\right]^{1/4} . \tag{2.2}$$

This length scale also sets a natural time scale $1/\Omega_0$, corresponding to a diffusion time needed for traversing this distance l_c,

$$\Omega_0=\frac{4D}{l_c^2}=(2\gamma g_2 D)^{1/2} . \tag{2.3}$$

Our key results can be stated in terms of these characteristic length and time scales.

The propagator G satisfies the above diffusion equation

$$\frac{\partial G(z,z',t)}{\partial t}=D\nabla_z^2 G(z,z',t) +i\gamma(g_1 z+g_2 z^2)G(z,z',t) , \quad t>0 \tag{2.4}$$

and, as usual,

$$G(z,z',t=0^+)=\delta(z-z') . \tag{2.5}$$

In this section we will consider an infinite system with the propagator going to zero, as the distances tend to infinity (homogeneous Dirichlet BC). The Green's function gives the local magnetization at z after time t for a packet initially concentrated at z'. Upon a simple shift of origin, this becomes the Green's function of a particle with an *imaginary* harmonic restoring force. The Green's function for the real harmonic force was worked out by Rayleigh, and it has a colorful history, which has been discussed by Kac.[23] A key difference between the cases for which an attractive potential is purely real (i.e., Rayleigh-Smoluchowsky) and the present case where it is purely imaginary is that there is no decay in the previous case, whereas there is decay in the present case. The operator on the right-hand side (rhs) of (2.4) also coincides with (minus) the Hamiltonian of a quantum-mechanical oscillator with imaginary potential. Using previously known results,[23,24] it is straightforward to show that the Green's function is equal to the following complex expression:

$$G(z,z',t)=\left[\frac{\Omega}{4\pi D\sinh\Omega t}\right]^{1/2}\exp\left[\frac{-\Omega}{4D}(z-z')^2\coth\Omega t-\frac{\Omega}{2D}\tanh\left[\frac{\Omega t}{2}\right]zz'\right] \times\exp\left\{i\gamma\frac{g_1}{\Omega}\tanh\left[\frac{\Omega t}{2}\right](z+z')-\frac{\gamma g_1^2 D}{\Omega^3}\left[\Omega t-2\tanh\left[\frac{\Omega t}{2}\right]\right]\right\} , \tag{2.6}$$

where the complex frequency Ω is given by

$$\Omega=(-4i\gamma g_2 D)^{1/2}=(1-i)\Omega_0 . \tag{2.7}$$

This Green's function can be verified by substitution. The total Green's function is obtained by multiplying the above equation by the free diffusion Green's function for directions x,y,

$$\hat{G}(\mathbf{r},\mathbf{r}',t)=G(z,z',t)\left[\frac{1}{4\pi Dt}\right]^{1/2}\exp\left[-\frac{(x-x')^2}{4Dt}\right]\left[\frac{1}{4\pi Dt}\right]^{1/2}\exp\left[-\frac{(y-y')^2}{4Dt}\right] , \tag{2.8}$$

which we write only for completeness but we need not consider. Similarly, it is straightforward to consider saddle points, since any quadratic magnetic field can be brought to a canonical form, for which Eq. (2.1) is separable, and can be obtained from the above Green's function.

It is useful to consider two limiting cases (i) $g_2=0$ and (ii) $g_2=g_1=0$. In the first case, taking $\Omega\to 0$ gives

$$G(z,z',t)\to\left[\frac{1}{4\pi Dt}\right]^{1/2}\exp\left[-\frac{(z-z')^2}{4Dt}+\frac{i}{2}\gamma g_1(z+z')t-\frac{(\gamma g_1)^2 Dt^3}{12}\right] , \quad g_2=0 \tag{2.9}$$

which is the Green's function in the presence of a uniform gradient, and which further reduces to the free propagator when $g_2=g_1=0$

$$G(z,z',t)\rightarrow\left[\frac{1}{4\pi Dt}\right]^{1/2}\exp\left[-\frac{(z-z')^2}{4Dt}\right],\quad g_1=g_2=0\ . \tag{2.10}$$

Since the Green's function (or the propagator) determines how the local magnetization evolves between the pulses, it contains all the information needed to compute the magnetization for any pulse sequence. A key feature of this propagator is that the magnetization creeps towards the center, i.e., the tip of the parabola. This is somewhat surprising, considering the fact that the potential is purely imaginary. In Fig. 2 we have plotted the absolute value of the Green's function, Eq. (2.6), without the preexponential $(\Omega_0/4\pi D)^{1/2}$ factor and for $g_1=0$ as a function of dimensionless distance $Z=z/(8D/\gamma g_2)^{1/4}$ at various dimensionless times $\tau=t(2\gamma g_2 D)^{1/2}$. The pulse starts as a δ function at $Z=1$ at $\tau=0$ and creeps toward the center of the parabola. In the long-time limit $\tau\rightarrow\infty$, we find

$$G(z,z',t)\rightarrow\left[\frac{\Omega}{2\pi D}\right]^{1/2}\exp\left[-\Omega\left[\frac{t}{2}+\frac{z^2+z'^2}{4D}\right]\right],\quad g_1=0\ . \tag{2.11}$$

The asymptotic form of the propagator has an overall decay in time and is a product of two Gaussian packets of characteristic size l_c, both centered around zero. In other words, contributions to the Green's function at a given point comes predominantly from distances l_c near the origin ($g_1=0$). Thus at long times the parabolic field acts as a local probe around the tip of the field with the characteristic size l_c. Clearly, l_c has to be smaller than any other length scales in the problem, for this conclusion to hold. Equation (2.11) should be contrasted against the propagator in an unbounded uniform gradient Eq. (2.9), which does not exhibit such an obvious characteristic size except from the diffusion length $(Dt)^{1/2}$.

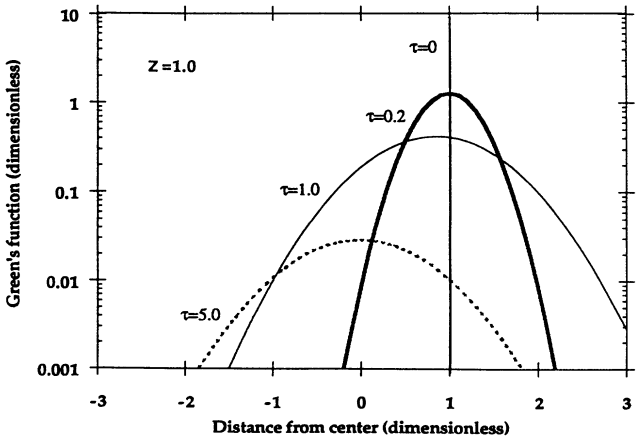

FIG. 2. Absolute value of the Green's function with $g_1=0$ as a function of dimensionless distance $Z=z/(8D/\gamma g_2)^{1/4}$ at various dimensionless times $\tau=t(2\gamma g_2 D)^{1/2}$. The pulse starts out as a δ function at $Z=1$ at $\tau=0$ and creeps toward the tip of the parabola.

The relation with the quantum-mechanical oscillator (in imaginary time) is also apparent in (2.11), which has the usual long-time form, dominated by the ground state:

$$G(z,z',t)\rightarrow\psi_0(z)\psi_0(z')\exp(-E_0 t)\ , \tag{2.12}$$

where $E_0=\Omega/2$ and $\psi_0(z)=(\Omega/4\pi D)^{1/4}\exp(-\Omega z^2/4D)$ are, respectively, the ground-state energy and wave function of the harmonic oscillator, analytically continued to imaginary potential. It is interesting that the most salient feature of the usual harmonic oscillator, e.g., the existence of a discrete spectrum of bound states, is preserved under the analytical continuation. The intriguing question of the nature of the spectrum for more general magnetic-field profiles is studied in more detail in Ref. 22.

If we think of a porous medium as a collection of hills and valleys of magnetic field, we can get a feeling for the magnitude of the length scales and time scales (see Fig. 1), by using an approximation[3] $g_1\sim$ (a geometrical factor)$\times\Delta\chi B_0/R_p$, where $\Delta\chi$ is the difference between the grain and the water susceptibility, R_p is the pore size. Similarly, $g_2\sim$ (a different geometrical factor) $\times\Delta\chi B_0/R_p^2$. So, when the geometrical factors are of order unity, we find the characteristic length is a geometrical mean of the pore size and a diffusion length l^*

$$l_c\sim(R_p l^*)^{1/2}\ ,\quad l^*=\left[\frac{D}{\Delta\chi B_0\gamma}\right]^{1/2}\ . \tag{2.13}$$

The diffusion length l^* corresponds to a diffusion distance over the time interval given by the inverse of the spread in Larmor frequency $\Delta\omega=\Delta\chi B_0\gamma$ arising from the field inhomogeneities. Using typical values of $\gamma B_0\sim 10$ MHz, $\Delta\chi\sim 10^{-5}$, the spread $\Delta\chi B_0\gamma$ is of the order of 100 Hz, which makes, using $D\sim 10^{-5}$ cm^2/s, l^* of order 3 μm. It is rather coincidental that in many porous media of interest, i.e., rocks, this is also a typical size of the pores. This also implies that $l_c\sim 3$ μm. A realistic model of a porous material should, in addition, include the effects of restricted diffusion and treat the wall effects in a realistic manner. This in itself is a difficult problem beyond the scope of this paper. The present estimates show that the effect of the *curvature* of the magnetic field can be as important as the effects of the walls, and should be included in any realistic theory for magnetization decay in rocks. Note that by varying B_0 or the susceptibility contrast $\Delta\chi$, l^* and hence l_c can be made either greater or smaller than R_p, which could allow for some experimental verification of the above arguments. To get a better idea on how the presence of the walls can modify the above arguments we will study in Sec. IV a somewhat artificial model of a pore of finite size and show that if the pore size $R_p\gg l_c$, the wall effects can be safely neglected. As we will see in Sec. V, the usual method of minimizing the field inhomogeneities is to apply spin-echo technique, such as the method of Carr and Purcell.[18] When the Carr-Purcell pulse spacing is

large compared to $1/\Omega_0$, which will happen if the internal gradients are large (e.g., at high B_0), the diffusion contribution to transverse relaxation overwhelms the wall relaxation mechanism[2] and T_2 becomes much shorter than T_1. This was pointed out by Kleinberg and Horsfield.[3]

III. ATTENUATION IN A PARABOLIC FIELD

In this section we obtain the solution for attenuation of the local magnetization following a $\pi/2$ pulse. In particular we find a crossover from a short-time $\exp(-t^3)$ behavior to a long-time $\exp(-t)$ behavior. The magnetization is obtained from its initial value $M(z,t=0)$:

$$M(z,t)=\int dz' G(z,z',t) M(z',0) \ . \tag{3.1}$$

Assuming that the initial magnetization is spatially uniform, integrating Eq. (2.6) over all z' gives

$$M(z,t)=\left[\frac{1}{\cosh\Omega t}\right]^{1/2} \exp\left[\frac{-\gamma^2 g_1^2 D}{\Omega^3}(\Omega t-\tanh\Omega t)+i\left[\frac{\tanh\Omega t}{\Omega}\right]\gamma(g_1 z+g_2 z^2)\right] , \tag{3.2}$$

where Ω is given by (2.7). In particular the absolute value is (in terms of real quantities):

$$|M(z,t)|=[\sinh^2(\Omega_0 t)+\cos^2(\Omega_0 t)]^{-1/4}\exp\left\{-\left[\frac{\Omega_0(z+g_1/2g_2)^2}{4D}\frac{\sinh(2\Omega_0 t)-\sin(2\Omega_0 t)}{\cosh(2\Omega_0 t)+\cos(2\Omega_0 t)}\right]\right\} . \tag{3.3}$$

We recall the definition $\Omega_0=(2\gamma g_2 D)^{1/2}$. Although in unbounded space g_1 is inessential, since it only produces a shift in the position of the tip of the parabola, we retain it in order to study the crossover in local magnetization.

We see immediately that, for $g_2=0$, we recover the well-known t^3 ultrafast-decay result[18,19]

$$M(z,t)=\exp(i\gamma g_1 z t)\exp\left[-\frac{D}{3}(\gamma g_1)^2 t^3\right] , \quad g_2=0 \tag{3.4}$$

which leads to the well-known result for the *effective* decay rate:

$$\frac{1}{T_2}=\frac{1}{T_{2B}}+\frac{D}{3}(\gamma g_1)^2 t^2 , \quad g_2=0 \ . \tag{3.5}$$

Note that for a uniform gradient the magnetization remains uniform.

The behavior of $M(z,t)$ will now be studied. In the short-time limit, it is always permissible locally to represent the field by an effective gradient, $g_1+2g_2 z$. Taking the limit $\Omega_0 t \ll 1$, we indeed find from Eq. (3.2)

$$M(z,t)\sim \exp i\gamma(g_1 z t+g_2 z^2 t+g_2 D t^2) \times\exp\left[-\left[\frac{D}{3}\gamma^2(g_1+2g_2 z)^2\right]t^3\right] . \tag{3.6}$$

The oscillatory terms of course denote a dephasing due to the local shift in the Larmor frequency. Note, however, that there is an extra oscillatory term due only to diffusion effect (see below). For short times the magnetization decays rapidly where the magnetic field varies rapidly spatially, and thus the magnetization becomes very rapidly inhomogeneous, leading to a totally different physics from the uniform gradient model.

In the long-time limit, $\Omega_0 t \gg 1$,

$$M(z,t)\sim\exp\left\{-\left[\frac{1}{2}(1-i)\Omega_0 t+\frac{\gamma g_2}{2\Omega_0}(1-i)\left[z+\frac{g_1}{2g_2}\right]^2-i\frac{g_1^2\gamma}{4g_2}t\right]\right\} . \tag{3.7}$$

We see that the magnetization decays exponentially, linearly in time, and uniformly in space, the final shape approaching a Gaussian distribution. We obtain the decay rate in an unbounded parabolic field:

$$\frac{1}{T_2}=\frac{1}{T_{2B}}+\left[\frac{\gamma g_2 D}{2}\right]^{1/2} , \tag{3.8}$$

where $g_2>0$ as previously discussed. Note that strictly speaking T_2 must be extracted from a spin-echo measurement, but here, as we show in Sec. V, it is also identical to the decay rate of the local magnetization (3.8). The shape of the asymptotic packet is a Gaussian of size l_c centered around the shifted tip of the parabola (at $z=-g_1/2g_2$), e.g., the extremum of the field. Since the last term in the exponential (3.7) is precisely the Larmor frequency corresponding to this extremum, an interesting feature of this long-time behavior is that due to diffusion there is an overall shift $\Omega_0/2$ with respect to the frequency of the minimum of the effective Larmor frequency, irrespective of the position. Thus the local magnetic inhomogeneity will also show up as a g shift. This shift, the exponential decay, and the Gaussian shape of the packet at long time are totally missed if the field were replaced by an effective gradient.

We display the above results graphically in Figs. 3–6, where for convenience we have set $g_1=0$. Around the tip of the parabola the t^3 term vanishes in the small-time expansion and instead one has

$$M(z,t)\sim\exp[i\gamma g_2 t(z^2+Dt)] \times\exp\left[-\frac{2D}{3}\gamma^2 g_2^2 t^3(Dt+2z^2)\right]. \quad (3.9)$$

Thus at $z=0$, the initial decay starts as t^4—which will also be true for distances smaller than the diffusion distance $(Dt)^{1/2}$. In Fig. 3 is shown the absolute value of the local magnetization as a function of the dimensionless time at the tip of the parabola (solid line). The initial decay is quite slow $\sim\exp(-\tau^4)$ (dashed line) and is slower than initial decay at other locations but eventually it becomes exponential (dotted line).

Figures 4 and 5 show the crossover from t^3 to t behavior in a region where the local gradient is nonzero ($Z=1,2$, respectively). An interesting feature is that for Z large enough (for large enough local gradient) the decay becomes *nonmonotonic,* so that in a certain time interval the local magnetization actually slightly increases. This feature is visible also on Fig. 2, but here it is more surprising since the initial magnetization is uniform. In Fig. 6 is plotted the absolute value of the local magnetization as a function of distance (dimensionless) from the tip of the parabola ($z=0$).

Thus, the physics of the parabolic field cannot be simulated by an effective uniform gradient. Bendel's[14] experiments, if carried out to longer times, would reveal the crossover to the linear regime (3.7) discussed above. The $\exp(-t^3)$ decay (3.5) which is often used in interpreting experiments is, in some sense, rather pathological and atypical, and can only be used as a guide for short times. The decay in any realistic system will rapidly cross over to a much slower exponential behavior. It is interesting

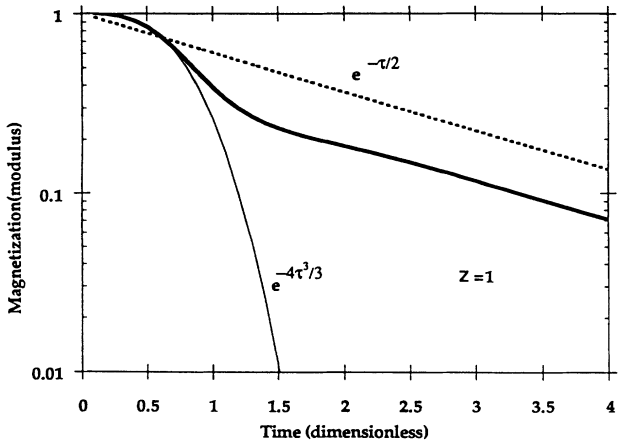

FIG. 4. Absolute value of the local magnetization at various dimensionless times at $Z=1$ (solid line). The initial decay is rather slow $\sim\exp(-\tau^3)$ (thin line), but eventually it becomes exponential (dotted line) ($g_1=0$).

to notice that the result (3.4) is somewhat unstable. For instance, using the Green's function (2.9), one finds that if the initial magnetization instead of being perfectly uniform has the form $M(z,t=0)=1+\epsilon\exp(-z^2/a^2)$, e.g., has a small localized fluctuation, the long-time decay of the local magnetization (for fixed z) becomes slower than (3.5) and equal to $\epsilon\exp[-(D/12)(\gamma g_1)^2 t^3]$. The total spin-echo amplitude, however, remains independent of the initial distribution of magnetization (see Sec. V). By contrast the long-time decay rate of the magnetization in a parabolic field is dominated by the ground state and thus is independent of the initial distribution.

While we have not incorporated the influence of real boundaries, partial results can be obtained for a semi-infinite system, i.e., a single wall, provided that some simple symmetries are maintained, so that method of images

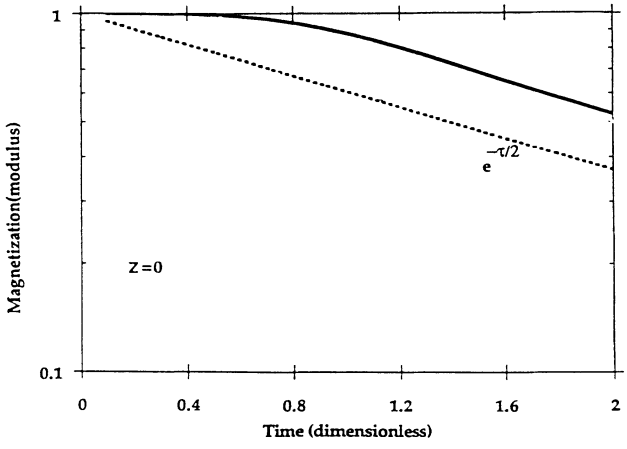

FIG. 3. Absolute value of the local magnetization at various dimensionless times at the tip of the parabola (solid line). The initial decay is rather slow $\sim\exp(-\tau^4)$ and is slower than initial decay at other locations, but eventually it becomes exponential (dotted line) ($g_1=0$).

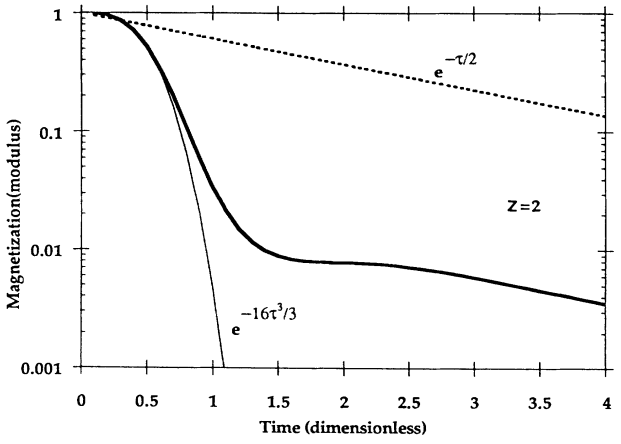

FIG. 5. Absolute value of the local magnetization at various dimensionless times at $Z=2$ (solid line). The initial decay is rather slow $\sim\exp(-\tau^3)$ (thin line), but eventually it becomes exponential (dotted line) ($g_1=0$).

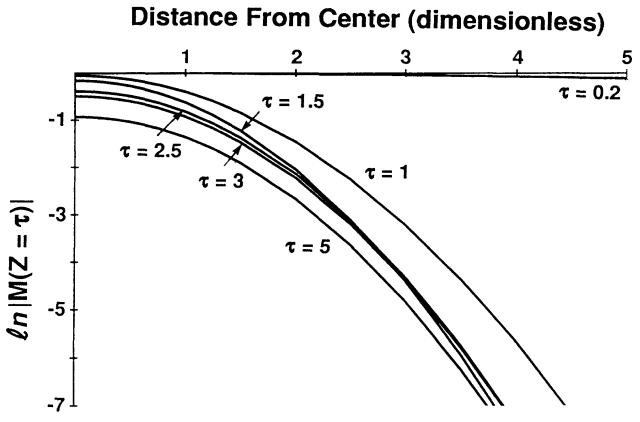

FIG. 6. Absolute value of the local magnetization as a function of distance (dimensionless) from the tip of the parabola at several different (dimensionless) times, showing that the decay is rapid away from the tip of the parabola, but decays slowly around the tip ($g_1=0$).

can be applied. An example of this is when the field minimum is at the wall, i.e., the wall is at $z=0$. Using the image method on the propagator (2.6) with $g_1=0$, one obtains the Green's function $G(z,z',t)+G(z,-z',t)$ for a reflecting wall and $G(z,z',t)-G(z,-z',t)$ for a perfectly absorbing wall ($\rho=\infty$). In the first case the wall does not change the asymptotic decay rate (although it slows the decay, since the amplitude is multiplied by 2), but in the second case T_2 is given by the first excited state of the harmonic oscillator and thus the decay rate, after subtracting the bulk, is three times (3.8).

IV. AN ARTIFICIALLY RESTRICTED DIFFUSION

In this section we compute the signal for a pulsed-field-gradient spin-echo (PFGSE) experiment in a parabolic field in the presence of an artificial restriction on diffusion. Since for typical experimental conditions l_c can be of the order of the pore size, it is important to understand the effect of the walls. A correct treatment of the additional effects of realistic walls is beyond the scope of this paper, but some of the effects of the boundaries can be understood by studying a solvable model where the diffusing spins are attracted to a center. As a result they are localized in a harmonic well of size R_p, which mimics restricted diffusion inside a pore. This model, without the parabolic field, was used by Stejskal[5] to study the influences of boundary on PFGSE. It mimics a boundary in the sense that the effective diffusion coefficient goes to zero, but it is a soft boundary since the density of spins goes continuously to zero at distances larger than R_p. Note also that confining the spins in a finite size removes some inessential problems of normalization when computing the total magnetization, which are associated with an infinite system. In this section we only compute the total PFGSE signal coming from a single pore. We will address the question of the total contribution coming from all pores in the next section when discussing the Hahn and CPMG echoes. Note that we find that the results of the previous sections hold when the pore size $R_p\to\infty$. Our main result is that the pore size is replaced by another effective size l_c.

In the presence of an attractive force $f=-2z/T$ the Torrey[19] equation has to be replaced by the following diffusion-convection equation for the Green's function with an extra attraction, denoted G_A:

$$\frac{\partial G_A(z,z',t)}{\partial t}=D\nabla_z^2 G_A(z,z',t)-\nabla_z\left[-2\frac{z}{T}G_A(z,z',t)\right]+i\gamma(g_1z+g_2z^2)G_A(z,z',t)\ , \tag{4.1}$$

with initial condition $G_A(z,z',t=0^+)=\delta(z-z')$. T is the diffusion time to traverse the sample $T=R_p^2/D$. Note that the attractive center is at $z=0$ but the tip of the parabola is at $z=-g_1/2g_2$, and that here g_1 cannot be removed by shifting, but represents the average gradient over the pore.

The following transformation:

$$G_A(z,z',t)=\exp\left[-\frac{1}{2DT}(z^2-z'^2-2Dt)\right]G(z,z',t)\ ,$$

brings Eq. (4.1) back to the form previously studied (2.4):

$$\frac{\partial G(z,z',t)}{\partial t}=D\nabla_z^2 G(z,z',t)+i\gamma(g_1z+g_2z^2)G(z,z',t)-\frac{z^2}{DT^2}G(z,z',t)\ . \tag{4.2}$$

Thus, the solution of the restricted diffusion model is simply related to the result derived in Sec. II, through

$$G_A(z,z',t)=\exp\left[-\frac{1}{2DT}(z^2-z'^2-2Dt)\right]\times G(z,z',t;\Omega\to\Omega_A)\ , \tag{4.3}$$

with the substitution

$$\Omega_A^2=\Omega^2+\frac{4}{T^2}\ . \tag{4.4}$$

In absence of external field inhomogeneities ($g_1=0,g_2=0$), G_A has a steady-state solution which mimics the presence of walls:

$$t\to\infty\ ,\quad G_A=\left[\frac{1}{D\pi T}\right]^{1/2}\exp\left[-\frac{z^2}{DT}\right]\ ,\quad g_1,g_2=0\ . \tag{4.5}$$

This is precisely the initial transverse magnetization when the $\pi/2$ pulse is applied. We should emphasize that the initial condition $M_A\propto\exp(-z^2/R_P^2)$ is not due to field inhomogeneity but is an approximation of a box function which is the characteristic function of the pore shape, i.e., a function which is unity in the pore and zero in the grain.[5] This Gaussian shape is meant to mimic a

magnetization which is uniform in the pore and which goes to zero sharply at the boundary.

Now we obtain the echo amplitude in a pulsed-field-gradient spin echo (PFGSE). The echo amplitude is given directly by the Fourier transform of the propagator with an average over the initial position. We have described the detailed formulation elsewhere.[21] Briefly, in a PFGSE experiment, a short pulse of a field gradient of duration δ and strength g_p is applied (in the z direction) to encode the spins. Then, the spins are allowed to diffuse for a time t after which the decoding is done by applying a short pulse of the same duration δ and strength but in the opposite direction $-g_p$. In the limit $\delta\to 0$, $|g_p|\to\infty$ with δg_p fixed, the expression for the decay amplitude, with the bulk decay $\exp(-t/T_{2B})$ factored out, is given by

$$M_A(k,t)=\int dz\,dz' G_A(z,z',t)e^{-ik(z-z')}M_A(z',0)\ , \qquad k=\gamma\delta g_p\ . \tag{4.6}$$

Here $k=\gamma\delta g_p$, and t is the time between the gradient pulses. Note that in order to keep the calculations simple we have not included a π pulse in the sequence considered here, and thus our result will be sensitive to inhomogeneous broadening as discussed below. The echo amplitudes which are of more direct experimental significance are also more complicated to compute and will be considered only in the next section. However, apart from some obvious modifications, most of the physics of the PFGSE is captured by the present calculation.

In the present case, we should take, from Eq. (4.5),

$$M_A(z',0)=\left[\frac{1}{D\pi T}\right]^{1/2}\exp\left[-\frac{z'^2}{DT}\right]\ . \tag{4.7}$$

The integrations are straightforward, albeit tedious, and give

$$M_A(k,t)=\left[\frac{\Omega_A T}{[1+(\Omega_A T/2)\coth(\Omega_A t/2)][1+(\Omega_A T/2)\tanh(\Omega_A t/2)]\sinh\Omega_A t}\right]^{1/2} e^{t/T} \times\exp\left[-\frac{\gamma^2 g_1^2 D}{\Omega_A^3}[\Omega_A t-2\tanh(\Omega_A t/2)]-\frac{\gamma^2 g_1^2 DT\tanh^2(\Omega_A t/2)}{\Omega_A^2[1+(\Omega_A T/2)\tanh(\Omega_A t/2)]}\right] \times\exp\left[-\frac{DTk^2}{1+(\Omega_A T/2)\coth(\Omega_A t/2)}\right]\ . \tag{4.8}$$

A. Meaning of restricted diffusion

Before we proceed to understand the above result, first let us explain the meaning of the artificial barrier using the limiting case of $g_1=g_2=0$, which corresponds to Stejskal's case.[5] In this case, $\Omega_A T=2$, and Eq. (4.8) gives

$$M_A(k,t)=\exp[-DTk^2(1-e^{-2t/T})/2]\ ,\quad g_1=g_2=0\ . \tag{4.9}$$

In the short-time limit, the exponent is Dk^2t, which corresponds to diffusion in an unbounded medium where the mean-square displacement is Dt. In a confined space, this can be at most the pore size squared, i.e., $R_p^2=DT$ in the long-time limit, i.e., the diffusion coefficient goes to zero in the long-time limit. However, there is a difference between the above magnetization and that in a system with real walls. In a pore with a real wall, the exponent contains higher powers of k^2, which reflects details of the pore geometry.[21] In this sense, the present model mimics an artificial boundary only by limiting the mean-square displacement. This model of attraction by a center has also another important property, discussed in more detail below, namely it is such that for $g_2=0, g_1>0$ the Gaussian phase approximation is exact for this model. This is because the solution of (4.1) with $g_2=0$ can be represented as an unrestricted Gaussian path integral in a standard way. This is why all the dependencies in g_1 that arise in the solution of this model are simple and analytic [typically as $\exp(-g_1^2)$, see (4.8)]. This model is actually the only model with bounded diffusion for which the Gaussian-phase approximation is exact.

B. Effective length in PFGSE

Now we consider the most important feature of Eq. (4.8), i.e., that the effective pore radius is l_c or R_p, whichever is smaller. To see this most clearly, let us consider the ratio $\ln[M_A(k,t)/M_A(0,t)]$, which is the usual quantity that is considered in the PFGSE experiments. This ratio denotes the excess attenuation by the pulsed gradient,

$$-\ln\frac{M_A(k,t)}{M_A(0,t)}=\frac{Dk^2T}{1+(\Omega_A T/2)\coth(\Omega_A t/2)}\ . \tag{4.10}$$

This result is independent of g_1, which would certainly not be correct for a real wall, and is an artifact of this simple model. However, as discussed below, it should be the correct result for small g_1. Now to see how the effective range crosses over from R_p to l_c, let us note that using the definition $R_p^2=DT$, $l_c^4=8D/\gamma g_2$, we can write

$$\Omega_A^2 T^2=4\left[1-8i\frac{R_p^4}{l_c^4}\right]\ . \tag{4.11}$$

When $R_p\ll l_c$, which implies $\Omega_A T=2$, Eq. (4.10)

reduces to Stejskal's result, i.e., confinement to R_p, which was discussed in the previous paragraph. As $\Omega_A T$ increases from its minimum value of 2, the size of l_c becomes more and more important, and for $R_p \gg l_c$, i.e., the pore size much greater than characteristic size, $\Omega_A T \gg 2$, Eq. (4.10) gives

$$-\ln\frac{M_A(k,t)}{M_A(0,t)}=\frac{2Dk^2}{\Omega_A}\tanh(\Omega_A t/2)\ , \tag{4.12}$$

which, in the short-time limit $\mathrm{Re}(\Omega_A)t/2 \ll 1$, exhibits free diffusion Dk^2t. But when $\mathrm{Re}(\Omega_A)t/2 \gg 1$, we find, using Eq. (2.3), that

$$-\ln\frac{M_A(k,t)}{M_A(0,t)}=\frac{2Dk^2}{\Omega_A}=\frac{k^2l_c^2(1+i)}{4}\ , \tag{4.13}$$

which reflects a confinement over a distance of order l_c. Again, we emphasize that the boundary is soft, since there are no higher powers of k^2 in Eq. (4.13).

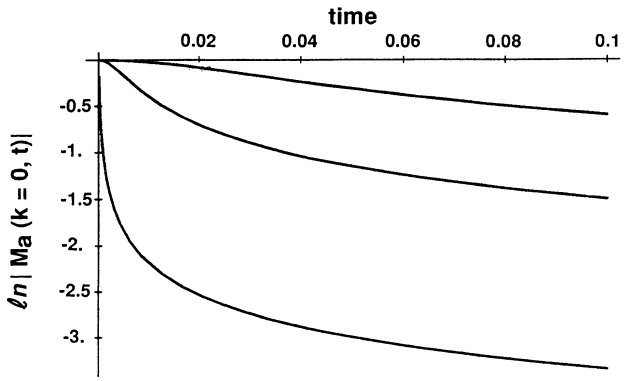

FIG. 7. Plot of $\ln|M_A(k=0,t)|$ as a function of t from Eq. (4.8) with dimensionless parameters $D=1, g_2=8$ (from top to bottom) $R_p=2,5,32$. In the units relevant for rocks (see Sec. V B), $D=2\times10^{-5}$ cm^2/s, $g_2=4\times10^7$ rad/s cm^2, and $R_p=28$, 70, and 450 μm, and times are in units of 100 ms.

C. The long-time behavior

Equation (4.8) has numerous interesting features and we will discuss a few of them. In Fig. 7 we have plotted $\ln|M(t,k=0)|$ as a function of t, for fixed g_2 and for several values of the pore size R_p. The behavior of $M(t,k)$ can be understood from various limiting cases: In the long-time limit, $\mathrm{Re}(\Omega_A)t \gg 1$, we find

$$M_A(k,t\to\infty)=\frac{(8\Omega_A T)^{1/2}}{2+\Omega_A T}\exp\left[-\frac{\Omega_A t}{2}+\frac{t}{T}-\frac{\gamma^2g_1^2D}{\Omega_A^2}\left[t-\frac{2}{\Omega_A(1+\Omega_A T/2)}\right]-\frac{Dk^2T}{1+\Omega_A T/2}\right]\ . \tag{4.14}$$

Now consider the case, $R_p \ll l_c$, which implies $\Omega_A T$ has its minimum value of 2.

$$M_A(k,t\to\infty)\approx\exp\left[i\frac{4R_p^4t}{l_c^4T}-\frac{1}{4D}\gamma^2g_1^2R_p^4t-\frac{1}{2}Dk^2T\right]\ . \tag{4.15}$$

From the linear time dependence of the exponent one could extract T_2 for this model, and this will be discussed in detail in the next section. For now, notice that the factor multiplying t is $T^2\sim R_p^4/D^2$. This form of $g_1^2R_p^4t/D$ is analogous to the results obtained by Robertson[20] and others[20] for a uniform gradient in a restricted geometry. This is not totally surprising since they use the Gaussian-phase assumption, which is exact for the present model for $g_2=0$ (but incorrect for real walls except in the limit of small g_1). Thus, we see that this approximation is also correct for $R_p \ll l_c$ (small g_2). When $R_p \gg l_c$ we find

$$M_A(k,t\to\infty)\approx\frac{2^{1/4}l_c}{R_p}\exp\left[i\frac{\pi}{8}-\frac{\Omega_0(1-i)t}{2}-\frac{i\gamma^2g_1^2Dt}{2\Omega_0^2}-\frac{(1+i)Dk^2}{\Omega_0}\right]\ . \tag{4.16}$$

Thus, the overall magnetization is down by a factor of effective pore radius by the true pore radius l_c/R_p, and the long-time limit shows that the decay rate is a nonanalytic function of g_2. It is clear that as long as $R_p/l_c \ll 1$, we can make a binomial expansion of Ω_A given by (4.11), and, therefore, for finite R_p the decay rate itself will be an analytic function of g_2. In the other extreme, $R_p/l_c \gg 1$, $\Omega_A\to\Omega=(1-i)(2g_2\gamma D)^{1/2}$ and hence the $g_2^{1/2}$ dependence of the decay rate, signaling the breakdown of the

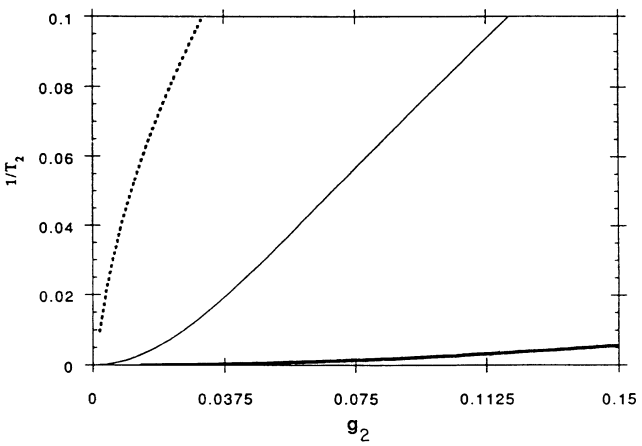

FIG. 8. $1/T_2$ shows a nonanalytic dependence on g_2 (in arbitrary units) for ratios of $R_p/l_c=5,2,1$ (from top to bottom).

Gaussian-phase approximation. The dependence of the rate on g_2 for various pore sizes is illustrated on Fig. 8, where one can see how rapidly the g_2^2 result predicted by the second-cumulant approximation becomes a very poor approximation.

D. The short-time behavior and inhomogeneous broadening

The short-time limit of the expression (4.8) is very instructive. Expanding (4.8) for $g_1=0$ and $k=0$ (total magnetization) one finds, substituting $T=R_p^2/D$,

$$M_A(k,t)=\exp\left[\frac{1}{3}DR_p^2\gamma^2g_2^2t^3-\frac{1}{3}D^2\gamma^2g_2^2t^4\left[1-i\frac{R_p^4\gamma g_2}{D}\right]+\cdots\right]$$

$$\times\exp\left[\frac{i}{2}R_p^2\gamma g_2t-\frac{1}{4}R_p^4g_2^2\gamma^2t^2-\frac{i}{6}R_p^3g_2^3\gamma^3t^3+\frac{1}{8}R_p^8\gamma^4g_2^4t^4+\cdots\right]. \quad (4.17)$$

Note that the second exponential, whose decay starts as t^2, is independent of D and thus originates only from inhomogeneous broadening inside a single pore. In fact this factor is exactly equal to the the total magnetization in the absence of diffusion:

$$M(k=0,t,D=0)=\int dz(\pi R_p^2)^{-1/2}\exp\left[-\frac{z^2}{R_p^2}\right]\exp(ig_2z^2t)=\frac{1}{(1-ig_2\gamma R_p^2t)^{1/2}}\ .$$

It is also this factor that is responsible for the sharp initial decay for large R_p of the curves of Fig. 7. The first exponential factor in (4.17), however, gives the decay coming from diffusion only (motional narrowing), and starts as t^3. At short times, the decay is controlled by the t^2 term, which arises from inhomogeneous broadening.

An interesting feature of (4.16) is the absence of inhomogeneous broadening at long times, e.g., the magnetization decay rate is not controlled by the overall linewidth within the parabola.

V. SPIN ECHOES

In the previous sections we obtained the solution for the attenuation of magnetization following a $\pi/2$ pulse, commonly called free-induction decay (FID). Experimentally, however, the FID is not a convenient way to measure the component T_{2D} of the rate of transverse magnetization relaxation arising due to diffusion in rocks. This is because when the internal field inhomogeneities are strong, the decay of the total magnetization is dominated by inhomogeneous broadening, e.g., by interferences between spins precessing at different Larmor frequencies at different points, which is a trivial effect independent of diffusion. For example, in Bendel's experiments on sand packs[14] inhomogeneous broadening is several hundred Hz. The detrimental effect of inhomogeneous broadening is removed by the spin-echo technique, where one π pulse (Hahn echo) or a series of π pulses [CPMG (Ref. 18)] are applied following the $\pi/2$ pulse. The purpose of this section is to show that the conclusions of the previous sections continue to hold for spin echoes. For the model of a parabolic field it is possible to compute exactly the echo amplitudes for the Hahn echoes and the Carr-Purcell sequence. Although the calculation does not present any conceptual difficulty, the algebra is very tedious and we will only discuss the main features in the text. The complete results and their derivation are summarized in the Appendix. Here we will first indicate how the echoes can be computed from the Green's function in general and in V A, as a useful reminder, we will illustrate on the simple example of the uniform gradient how the echo technique removes the effect of the inhomogeneous broadening. In V B we will analyze in detail the result for T_2, extracted from the Hahn-echo experiment, and how it compares with experimental data in rocks. In V C we will analyze the results for a CPMG pulse sequence and draw some comparison with the experimental data of Kenyon.[17] In V D we discuss the comparison with Bendel's[14] experiments.

This calculation also gives some information about a collection of pores. Indeed, when echo amplitudes are real [e.g., CPMG for odd echoes $2t_1,6t_1,\ldots$, see Eqs. (A1) and (A2)], the amplitudes corresponding to different pores do not interfere with each other, and thus there is no further inhomogeneous broadening effect when adding contributions from many pores (for even echoes, the effect is small). Thus it is not unreasonable to use the following results valid for a single pore to draw conclusions for a collection of such pores, at least on intermediate-time scales such that the interpore diffusion can be neglected, i.e., $t\ll R_p^2/D$.

Following a $\pi/2$ pulse, the total magnetization is obtained from its initial value $M(z,0)$:

$$M(t)=\int dzM(z,t)=\int dz\,dz'G(z,z',t)M(z',0)\ , \quad (5.1)$$

which we will write in a matrix notation as

$$M(t)=\int dz\,dz'\langle z|G(t)M(0)|z'\rangle\ .$$

Whereas $\langle z|M(0)|z'\rangle=M(z,0)\delta(z-z')$ has diagonal ele-

ments, $\langle z|G(t)|z'\rangle = G(z,z',t)$ has off-diagonal elements as well and is the propagator calculated in Sec. II or, in the presence of an artificial boundary in Sec. IV [G should than be replaced by G_A given by (4.3) and (4.4)]. Now the effect of a π pulse at time t_1 is to change the magnetization to its complex conjugate. Then, at time $t > t_1$, the observed magnetization or Hahn-echo signal (or first Carr-Purcell echo) is given by

$$M_H(t) = M_{\mathrm{CP1}}(t) = \int dz\, dz' \langle z|G(t-t_1)G^*(t_1)M(0)^*|z'\rangle \ . \quad (5.2)$$

This amplitude reaches a sharp maximum, or echo, at $t = 2t_1$, where it is measured (see below). The measured Hahn-echo signal is thus $M_H(t=2t_1)$ and one is interested in its decay rate T_2^{-1} as a function of $t = 2t_1$. Similarly the Carr-Purcell–echo sequence is obtained by applying a succession of π pulses at times $t_1, 3t_1, 5t_1, \ldots$, and measuring the corresponding echoes at times $2t_1, 4t_1, 6t_1, \ldots$. Using this matrix notation it is simple to write the measured amplitudes for the pulse sequences. For example,

$$\begin{aligned} M(4t_1) &= \int dz\, dz' \langle z|G(t_1)G(2t_1)^*G(t_1)M(0)|z'\rangle \ , \\ M(6t_1) &= \int dz\, dz' \langle z|G(t_1)G(2t_1)^*G(2t_1)G(t_1)^*M(0)^*|z'\rangle \ , \end{aligned} \quad (5.3)$$

and usually one plots the magnetization at the nth echo ($n = t/2t_1$), as a function of t for fixed t_1. One expects for large t

$$M(t = 2nt_1) \sim \exp[-t/T_2(t_1)] \ , \quad (5.4)$$

which defines an effective decay rate $T_2(t_1)^{-1}$ for fixed pulse spacing. The standard definition of T_2 is that when $t_1 \to \infty$, $T_2(t_1) \to T_2$ (see below).

A. Spin echoes and inhomogeneous broadening, $g_2 = 0$

To illustrate how the echo technique suppresses inhomogeneous broadening consider now the simple case of the uniform gradient $g_2 = 0$ in unbounded space (e.g., in a box of size $2L$, very large compared to the diffusion length). By integration of (3.4) one finds that the total magnetization, or FID amplitude, is given by

$$M(t) = \frac{1}{2L}\mathrm{Re}\int_{-L}^{L} dz\, M(z,t) \ , \quad (5.5)$$

which gives

$$M(t) = \frac{\sin\gamma g_1 L t}{\gamma g_1 L t}\exp\left[-\frac{D}{3}(\gamma g_1)^2 t^3\right] \ . \quad (5.6)$$

One should remember that for measured quantities in the laboratory coordinates the above expressions should be multiplied by $\cos(\omega_0 t)\exp(-t/T_{2B})$. We have taken $M(0) = 1/(2L)$. The first term of Eq. (5.6) is a decaying oscillatory term which is due to inhomogeneous broadening and exists even if $D = 0$. If $\gamma g_1 L T_2 \gg 1$, it completely dominates the signal and makes direct measurement of T_2 difficult. Let us now compute the first Hahn-echo amplitude for the same model. Inserting the propagator (2.9) in (5.3) one obtains

$$M_H(t) = \frac{\sin\gamma g_1 L(t-2t_1)}{\gamma g_1 L(t-2t_1)} \times \exp\left[-\frac{D}{3}(\gamma g_1)^2[t_1^3 + (t-t_1)^3]\right] \ . \quad (5.7)$$

At $t = 2t_1$, the first term becomes unity and thus the pulse height can be used to extract the decay rate T_2 and D, which may not be possible from examining the FID, Eq. (5.6). Note we have neglected the simultaneous influence of the boundary and diffusion in the above calculation. A similar calculation for the CPMG pulse sequence shows that the echo amplitude at time $t = 2nt_1$ is

$$\begin{aligned} M(t = 2nt_1) &= \exp[-(D\gamma^2 g_1^2 t^3/12n^2)] \\ &= \exp[-(D\gamma^2 g_1^2 t_1^2 t/3)] \ , \end{aligned} \quad (5.8)$$

a result which was obtained by Carr and Purcell.[18,19]

B. Hahn-echo amplitude and T_2, $g_2 \neq 0$

The Hahn-echo amplitude can be computed from (5.2) as sketched out in the Appendix. The full expression valid at all times is obtained from (A8) by integration as indicated in (A7). Here we will discuss only the short-time limit, and the long time (e.g., the determination of T_2). The intermediate-time regime, the shapes of the decay curves, and comparison with Bendel's experiments will be discussed in Sec. V D.

First consider the long-time limit. At long times the Green's function G_A of (4.3) takes the following form, dominated by the ground state:

$$G_A(z,z',t) \to \exp\left[-\frac{z^2}{2DT}\right]\psi_0(z)\exp(-E_0 t)\psi_0(z') \times \exp\left[\frac{z'^2}{2DT}\right] \ , \quad (5.9)$$

where

$$\psi_0(z) = \left[\frac{\Omega_A}{4\pi D}\right]^{1/4}\exp\left[-\frac{\Omega_A z^2}{4D} + i\frac{\gamma g_1}{\Omega_A}z + \frac{\gamma g_1^2 D}{\Omega_A^3}\right] \quad (5.10)$$

is the ground-state wave function, and

$$E_0=\frac{\Omega_A}{2}-\frac{1}{T}+\frac{\gamma^2 g_1^2 D}{\Omega_A^2} \tag{5.11}$$

is the ground state energy. We can now use (5.3) and the initial magnetization (4.7) and obtain the Hahn echo at time $t=2t_1$ for large pulse spacing t_1 as

$$M_H(t)\sim Ae^{-\mathrm{Re}(E_0)t}, \tag{5.12}$$

where the preexponential amplitude can be obtained simply in terms of the ground-state wave function $\psi_0(z)$:

$$A=\int dz|\psi_0(z)|^2\left|\int dz\frac{1}{(\pi DT)^{1/4}}e^{-z^2/2DT}\psi_0(z)\right|^2 . \tag{5.13}$$

We have thus obtained T_2 from the Hahn echo as $\mathrm{Re}(E_0)$:

$$\frac{1}{T_2}=\frac{1}{T_{2B}}+\mathrm{Re}\left[\frac{\Omega_A}{2}-\frac{1}{T}+\frac{\gamma^2 g_1^2 D}{\Omega_A^2}\right] . \tag{5.14}$$

This result is the same as the long-time FID decay from (4.14).

For intermediate times the excited states will contribute and the decay will appear as a superposition of exponentials, as clear from the figures discussed.

We now analyze this result for T_2 and show that it leads to reasonable values for rocks. Let us define the rate coming only from diffusion:

$$\frac{1}{T_2}=\frac{1}{T_{2B}}+\frac{1}{T_{2D}} . \tag{5.15}$$

To understand the relative importance of the contributions of the curvature and of the average gradient, and the different regimes it is natural to introduce the two dimensionless parameters:

$$\tilde{g}_2=\frac{\gamma g_2 R_p^4}{D}=\frac{8R_p^4}{l_c^4}, \quad \tilde{g}_1=\frac{\gamma g_1 R_p^3}{D} \tag{5.16}$$

in terms of which (5.14) takes the simple form

$$\frac{1}{T_{2D}}=\frac{D}{R_p^2}\left[F[\tilde{g}_2]+\frac{\tilde{g}_1^2}{4}G[\tilde{g}_2]\right], \tag{5.17}$$

where

$$F[u]=\left[\frac{1+(1+u^2)^{1/2}}{2}\right]^{1/2}-1 ,$$
$$G[u]=\frac{1}{1+u^2} . \tag{5.18}$$

As previously noted the dependence in the average gradient g_1 is simple and structureless, which is an artifact of the model with soft walls (see below).

The decay rate is plotted in Fig. 9 as a function of the dimensionless curvature parameter $\tilde{g}_2=8R_p^4/l_c^4$ for different values of the dimensionless average-gradient parameters $\tilde{g}_1$ (we have chosen $R_p=1$ and $D=1$ and the natural units for rocks are explained below). In the small

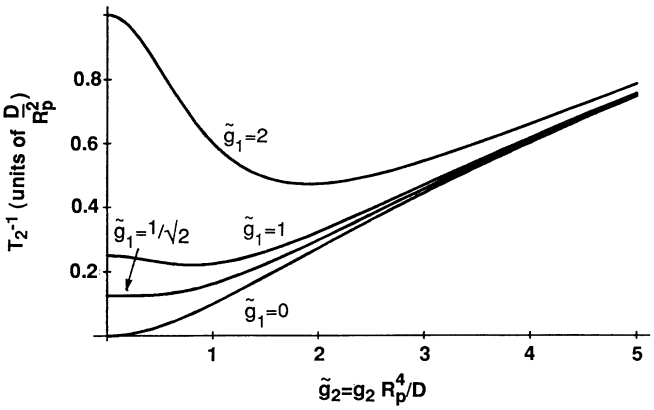

FIG. 9. Plot of $1/T_2$ in units of D/R_p^2 from (5.17) as a function of the dimensionless curvature $\tilde{g}_2$, for different values of the dimensionless gradient $\tilde{g}_1$.

$\tilde{g}_2$ regime ($R_p \ll l_c$) the effects of the curvature are weak and one has (expanding $F[u]\sim u^2/8$)

$$\frac{1}{T_{2D}}=\frac{\gamma^2 g_2^2 R_p^6}{8D}+\frac{\gamma^2 g_1^2 R_p^4}{4D} . \tag{5.19}$$

This expression is quadratic in the derivative of the field and thus is identical to the result of the Gaussian-phase approximation for this model. The standard cumulant expansion would give higher-order terms in g_1 and g_2. It is clear in Fig. 9 that the range of validity of (5.12) is very limited. In the large-u limit, e.g., for fixed average gradient and strong curvature, $F[u]\sim(u/2)^{1/2}$ and $G[u]\sim 1/u^2$ and thus the influence of both the gradient and the boundary becomes negligible and one recovers the result (3.8) for T_2 in an unbounded parabolic well:

$$\frac{1}{T_{2D}}=\left[\frac{\gamma g_2 D}{2}\right]^{1/2} . \tag{5.20}$$

Finally, when $\tilde{g}_2$ takes intermediate values, we observe on Fig. 9 that for large enough average gradient the decay rate exhibits a minimum as a function of $\tilde{g}_2$ (the minimum exists for $\tilde{g}_1>2^{-1/2}$).

What are the order of magnitudes of these effects in rocks? To facilitate the comparison with rock data, we note that the decay rates range from 20 to 200 s^{-1}, thus $\tau=100$ ms makes a convenient unit of time. With the diffusion coefficient of water (we take $D=2\times10^{-5}$ cm^2/s) the unit of length is $a=(D\tau)^{1/2}\sim 14$ μm. In these units the decay rates in rocks vary widely, but we can take 2–20 as a typical range. Note that in these units D is 1. For other systems such as gases, the present results can be used by simply changing the units in order to make the new D equal to 1. We use the same assumption as in Sec. II, e.g., that R_p sets the scale for the field inhomogeneities. Let us first consider a pore with zero average gradient, $g_1=0$. From Sec. II, the curvature of the field is

$$\gamma g_2=\Phi_2\frac{\gamma\Delta\chi B_0}{R_p^2} , \tag{5.21}$$

where Φ_2 is a geometrical factor. For $\gamma B_0 = 10$ MHz, $\Delta\chi = 10^{-5}$ we have, in units defined above, $\gamma g_2 = 2\pi\Phi_2 \times 10/R_p^2$. Since Φ_2 is unknown and since one can also vary the external field and consider different grain contrast, we have plotted in Fig. 10, T_2, given by (5.16), as a function of the pore size R_p using several different relations, $g_2 = 3/R_p^2$, $g_2 = 10/R_p^2$, $g_2 = 30/R_p^2$, respectively, which lead to increasing decay rates. Note that the decay rate has a maximum for pores of about 4–10 μm and attains values which are comparable with values measured in rocks, certainly for those with the slower decay rate. Equation (5.21) is, in fact, a conservative assumption because the local curvature of the field might be determined by smaller length scales (grain surface, etc.), in which case Φ_2 can be larger, leading to faster decays. In reality, each pore will probably also have an average gradient and we have represented in Fig. 11 the additional effect of a gradient $g_1 = 0, 3/R_p, 10/R_p$, respectively, for the central value of Fig. 10, $g_2 = 10/R_p^2$.

In the short-time limit, one can obtain from (A8)

$$M_H(t = 2t_1) \sim \exp(-\tfrac{4}{3} D\gamma^2 g_2^2 R_p^2 t_1^3) \tag{5.22a}$$

for $g_1 = 0$. To lowest order this is identical to the usual t^3 decay in a uniform effective gradient provided this effective gradient is taken to be equal to the average of the square of the local gradient [the average is over the initial distribution (4.7)]. This agrees with the general result of Tarczon and Halperin,[11] which was obtained using the Gaussian-phase approximation. As expected, this approximation is valid at very short times (or for very small g_2, see above). Note, however, that the small-t expansion is singular when $R_p \to \infty$ (with fixed g_2). To see that consider again the unbounded parabola model of Secs. II and III ($R_p = \infty$). Assuming, as in Sec. III, a uniform density unity over the whole space at $t = 0$ (and thus infinite initial total magnetization), one gets from (5.2) and (3.2), the exact result:

$$M_H(t = 2t_1) = |\cosh\Omega t_1|^{-1} \left[\frac{2\pi D}{\mathrm{Re}\,(\Omega \tanh \Omega t_1)} \right]^{1/2} . \tag{5.23}$$

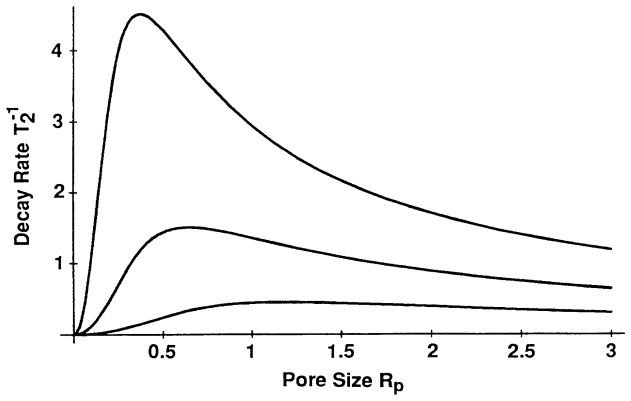

FIG. 10. Plot of $1/T_2$ as a function of the pore size. For rocks, the unit of length is 14 μm and the unit of time is 100 ms for various geometrical factors (see the text), and $g_1 = 0$.

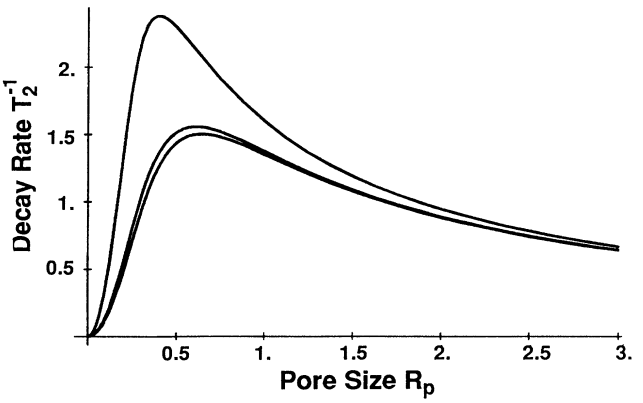

FIG. 11. Plot of $1/T_2$ as a function of the pore size. For rocks, the unit of length is 14 μm and the unit of time is 100 ms for various $g_1 \neq 0$, see the text.

The total Hahn-echo amplitude becomes finite for any $t_1 > 0$ because of the rapid decay in the regions far away from the tip of the parabola where the gradients are arbitrarily large. Since the initial magnetization is infinite, (5.23) diverges for small t_1 as in $l_c^4/(Dt_1)^{3/2}$. Although this divergence is an artifact of the unbounded parabola model, which, by itself, is an unphysical model, it has interesting consequences for the case where R_p is finite but large and where the total initial magnetization is chosen to be unity, i.e., the density of magnetization is $1/R_p$ rather than unity. Then from (5.23) one learns that in that case there are really two short-time (within $t_1 \ll 1/\Omega_0$) regimes: either $D\gamma^2 g_2^2 R_p^2 t_1^3 \ll 1$ and (5.22a) is correct, or $D\gamma^2 g_2^2 R_p^2 t_1^3 \gg 1$ and, from (5.23),

$$M_H(t = 2t_1) \sim \frac{l_c^4}{R_p (Dt_1)^{3/2}} , \tag{5.22b}$$

where we have divided (5.23) by a factor R_p, since, now the total initial magnetization is unity. This illustrates that for fixed g_2 the order of the limits $t_1 \to 0$ and $R_p \to \infty$ must be treated carefully, and shows that for large R_p and fixed g_2 (e.g., when large regions of high local gradients exist in the system), formula (5.22a) is of limited validity.

To assess the relative importance of the gradient of the field versus its curvature, it is useful to define locally a length scale $l(z) = g_1(z)/g_2(z)$ in terms of the local gradient $g_1(z)$ and consider the local Hahn-echo amplitude restricted to walks starting at z (the total amplitude being simply the sum of the local amplitudes over z, weighted by the initial magnetization). For short times, the decay is given by the effective gradient, as in (5.22a), but where now both g_1 and g_2 come into play [as, for example, in Eq. (3.6), which contains the total local gradient $g_1 + 2g_2 z$]. But when $\Omega_o t \gg 1$, the decay is determined by $\exp[-(\Omega_0 t)]$ term. This is because the long-time behavior is dominated by the lowest eigenfunction, as discussed above, which is sensitive to the curvature only. Note that when the crossover between the two (short- and long-time) regimes occurs the local Hahn amplitude

is of order $\exp[-l(z)^2/l_c^2]$. Thus only the points near the extrema that are within a distance $l(z)<l_c$ [i.e., the local length scale $l(z)$ is of order l_c or smaller], will determine the decay of the total amplitude after that time $t>1/\Omega_0$.

C. CPMG pulse sequence

For the ordinary Carr-Purcell sequence in an unbounded uniform gradient the pulse height is $\exp[-(D\gamma^2 g_1^2 t_1^2 t/3)]$. Thus, when $\ln M_{CP}(t)$ is plotted as a function of t, the envelope curves for different spacings t_1 should be straight lines intersecting at the origin and separating from each other due to their different slopes $\sim t_1^2$. Experimental data of Bendel[14] on sand packs and Kenyon[17] on rocks show quite a different picture: (i) The decay curves have noticeable curvature at short times: the initial decay is much faster than the long-time decay. (ii) The observed separation among the curves corresponding to different pulse spacing is a much weaker function of the pulse spacing than t_1^2, which is predicted by the above equation. Attempts have been made to explain these deviations from the unbounded uniform gradient picture. Kenyon[17] could reproduce decay curves with some curvature by using superposition of curves for decay in an unbounded uniform gradient, but with different strengths and weights. Kleinberg and Horsefield[3] pointed out that one should include more properly the effect of the boundary, but also assumed that the local inhomogeneous field can be represented by a uniform gradient. They used the results of Neumann,[20] which assume that the phases have a Gaussian distribution and furthermore, they extended Neumann's calculation for a sequence of pulses using the assumption that the magnetization remains uniform. They[3] pointed out that the gradient g_1 needed to explain the data was too high.

We have computed the pulse height for the CPMG sequence for the parabolic field model with artificially restricted diffusion. The calculation can be found in the Appendix. Let us discuss the main results as illustrated on Figs. 12–16.

(i) The slopes $1/T_2(t_1)$, as defined by (5.8), are shown in Fig. 12 using Eq. (A17) normalized by its asymptotic value for zero average gradient and various values of the pore size. The small-time behavior is found to be

$$1/T_2(t_1)\sim\frac{2D\gamma^2 g_2^2 R_p^2}{3}t_1^2 . \tag{5.24}$$

This equals to (5.8) with g_1^2 replaced by the average of the squared gradient. However, a very noticeable feature is that this initial t_1^2 behavior holds only for very small t_1, and is rapidly replaced by a linear behavior, and finally saturates to a constant value independent of t_1, which is in agreement with the observations of Kenyon.[17] More precisely, in the small-$\tilde{g}_2$ regime (weak curvature) this saturation can be accounted for by replacing t_1 in the above expression by R_p^2/D recovering formula (5.19). But this holds only for very small $\tilde{g}_2$ for, as soon as $\tilde{g}_2$ takes intermediate or large values the above substitution is not correct because l_c is now the relevant length. For large $\tilde{g}_2$, one would have to replace t_1 by l_c^3/DR_p, a choice not obvious *a priori*. One can show that for large t_1, $1/T_2(t_1)\sim 1/T_{2D}-C/t_1$, where C is related to the ground-state wave function (see the Appendix). Thus the approach to the asymptotic value is relatively slow (not exponential), which is also in agreement with some experimental observations. It is interesting to note that in the unbounded parabolic field ($R_p=\infty$) the packet at large time t also takes a Gaussian shape, but now characterized by a length scale $l_c(t_1)>l_c$, which crosses over to l_c as $t_1\to\infty$. This effective length scale is plotted in Fig. 13 [from formula (A15)]. $l_c(t_1)>l_c$ because the repeated refocusing by CPMG pulses reduces the effect of regions of high local gradients, thus reducing the effective curvature of the field inhomogeneities. Finally Fig. 14 is a plot of

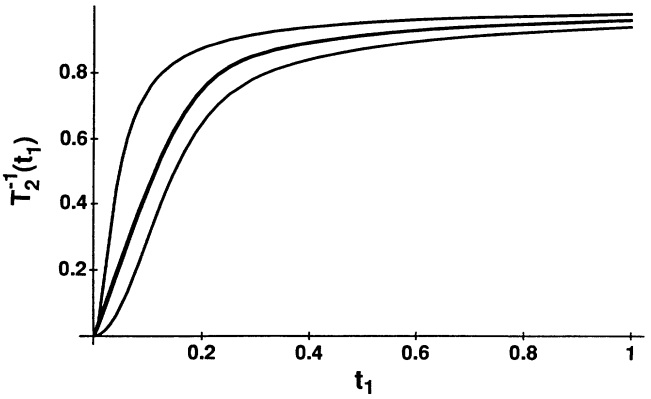

FIG. 12. Plot of $1/T_2(t_1)$ from (A17), normalized to its asymptotic value $1/T_2$, as a function of pulse spacing t_1, for $g_1=0$, and dimensionless parameters $D=1$, $g_2=8$ for $R_p=1$ (lower curve), $R_p=5$, $R_p=0.3$. In the units relevant for rocks (see Sec. V B), $D=2\times10^{-5}$ cm^2/s, $g_2=4\times10^7$ rad/s cm^2, and $R_p=14$, 70, and 4.4 μm, and times are in units of 100 ms.

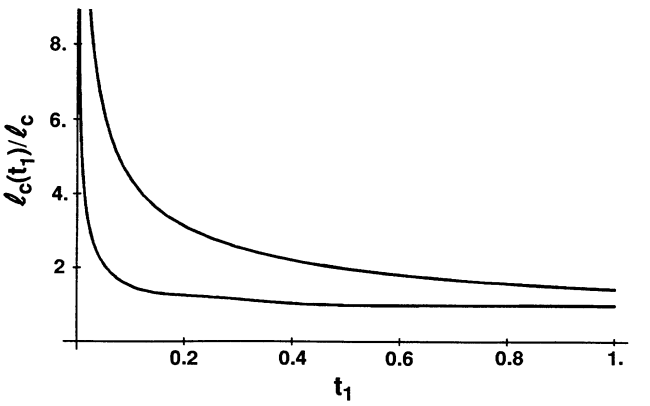

FIG. 13. Size of the magnetization packet $l_c(t_1)/l_c$ for a CPMG experiment in an unbounded parabolic field as a function of pulse spacing t_1, in units of 100 ms. The upper curve is for $g_2=4\times10^7$ rad/s cm^2, and the lower one for $g_2=5\times10^8$ rad/s cm^2.

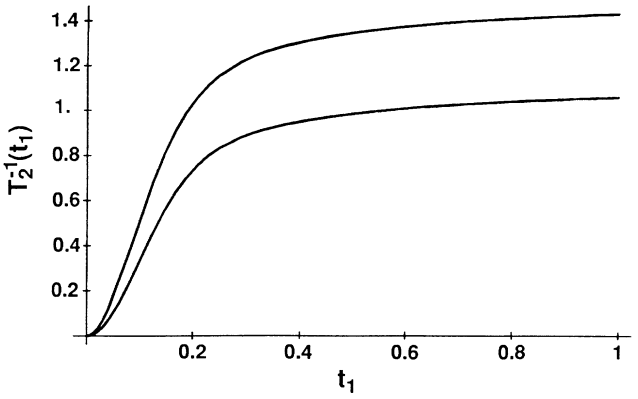

FIG. 14. Same as Fig. 12, but with an additional effect of a gradient. Plot of $1/T_2(t_1)$ from (A18) for $g_1=0$ (lower curve) normalized to the asymptotic value and $g_1=10$ as a function of pulse spacing with the same g_2 as in Fig. 12 and $R_p=1$. In the units relevant for rocks (see Sec. V B), $D=2\times10^{-5}$ cm^2/s, $g_2=4\times10^7$ rad/s cm^2, $g_1=7\times10^4$ rad/s cm, and $R_p=14$ μm, and times are in units of 100 ms.

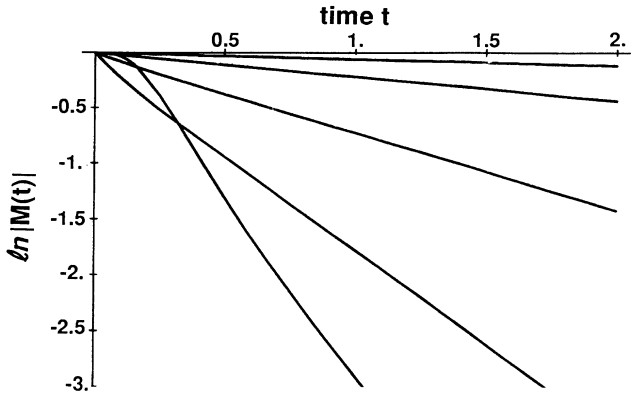

FIG. 16. $\ln|M(t)|$ as a function of t for CPMG envelope for various $t_1=1$, 2, 4, and 8 ms (from top to bottom); the lowest curve is the second echo envelope for $t=4t_1$. The unit of time is 100 ms. The pore size is 14 μm and $g_2=1.6\times10^8$ rad/s cm^2. Corresponding curves for other pore sizes can be obtained by rescaling g_2, t as described in the text.

Eq. (A18) and shows the additional effect on $T_2(t_1)$ of adding an average gradient.

(ii) We also computed the complete decay curves for an arbitrary number of echoes as a function of t and for various spacings t_1. The calculation shows that in general there is indeed a curvature in the curves of $\ln[M(t)]$ vs t, for fixed t_1 as observed by Kenyon, i.e., the initial slope is higher. We find roughly two different regimes, illustrated in Fig. 15 and Fig. 16, respectively. Figure 15 shows the CPMG curves for $g_2=100$, $R_p=5$ in the units discussed above in Sec. IV B. The rapidly decaying curve is the *second* Hahn echo (at $t=4t_1$). For these values of the parameters there is a rapid initial decay and a noticeable curvature. Although these values reproduce quite well

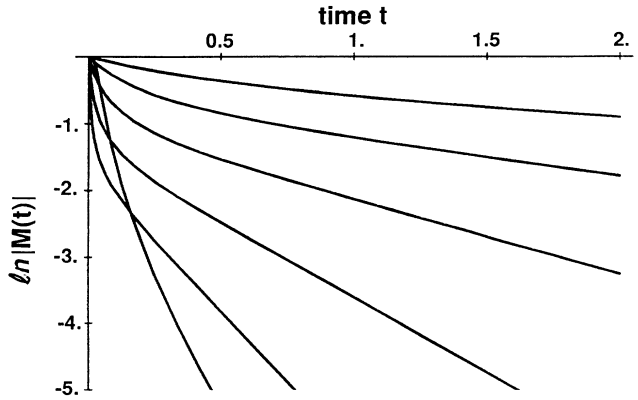

FIG. 15. $\ln|M(t)|$ as a function of t for CPMG envelope for various $t_1=0.25$, 0.5, 1, 2, and 4 ms (from top to bottom); the lowest curve is the second echo envelope for $t=4t_1$. The unit of time is 100 ms. The pore size is 70 μm and $g_2=5\times10^8$ rad/s cm^2. Corresponding curves for other pore sizes can be obtained by rescaling g_2, t as described in the text.

Kenyon's data for rocks with higher decay rate (the T_2 for Fig. 15 is around 7), they cannot be reconciled with the simple assumption (5.21) that R_p sets the length scale for the curvature (Φ_2 would be very high). Instead the data correspond to a parabolic field with strong curvature in an almost unbounded pore. Thus, it seems that the fast initial decay is due to the volume reduction effect, e.g., that most of the magnetization becomes concentrated in a small region, Eq. (5.23). There is some resemblance with the situation in Fig. 7, which, however, was due to inhomogeneous broadening. If one were to use, instead, the estimate (5.21) one would obtain a set of curves looking like those in Fig. 16 (plotted for $g_2=30$, $R_p=1$), e.g., almost straight lines. As previously noted (5.21) is a conservative assumption. The quantitative prediction of this very simplified model cannot completely explain the data, since there are many other sources of decay in rocks, such as the killing factor at the boundary.

(iii) Often in the literature,[3] a simple product rule is used to compute the CPMG echoes. In this rule, the time dependence of the local magnetization is assumed to factor and is independent of the space dependence. As a result, the decay of the local magnetization in the FID can be used to compute the echoes. The present calculation reveals that, except in some limiting cases (t_1 becomes very large, etc.) the product rule becomes incorrect as soon as the magnetization becomes inhomogeneous (it actually breaks down simultaneously with the Gaussian-phase approximation). Also, note that the CPMG echoes are not all purely real, and thus some additional interference effects are expected (see the Appendix for details). However, the echo amplitudes are almost real, so, we expect this effect to be small.

D. Comparison with Bendel's (Ref. 14) data

As we noted in the Introduction, Bendel[14] studied (i) diffusion in a very large sample (5.8 cm) subjected to an

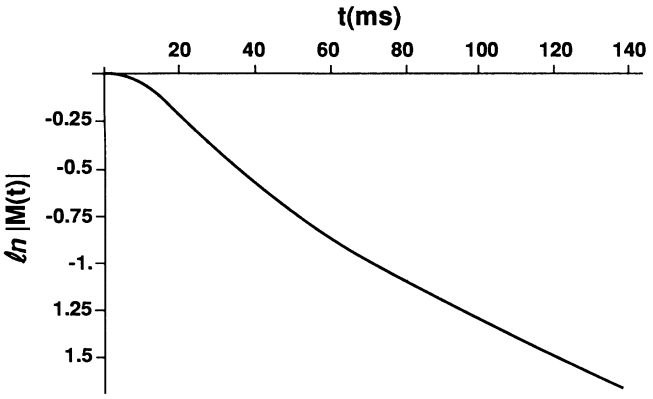

FIG. 17. $\ln|M(t)|$ as a function of t for the second Hahn echo envelope for $t=4t_1$. The parameters, which correspond to Bendel's experiment on sand packs, are given in the text.

externally applied parabolic field (ii) in a sand pack. For the first experiment, Bendel[14] gives $\gamma g_2=1150$ rad/s cm^2. From that we find that $1/\Omega_0$ in Eq. (2.7) is about 5 s. It is not surprising, as we have shown here, Eqs. (5.22) and (5.23), that the short-time (i.e., ≤ 1 s) data can be fitted by a distribution of gradients. However, for times longer than a few seconds one should observe a crossover to a linear regime. Also we suggest that a nonanalytic dependence on g_2 could be observed from the long-time decay rates.

Data on sand packs reveal a strong departure from the model of Bendel,[14] which uses a distribution of gradients. The reported inhomogeneity $\Delta\omega/2\pi$ is a few hundred Hertz. The particle size is about 1 mm in diameter so the pore size is about 170 μm. Using Eq. (5.21) with a geometrical factor of 2 gives $g_2=2\times10^7$ rad/s cm^2. This gives a $1/\Omega_0$ in Eq. (2.7) of about 50 ms, which coincides

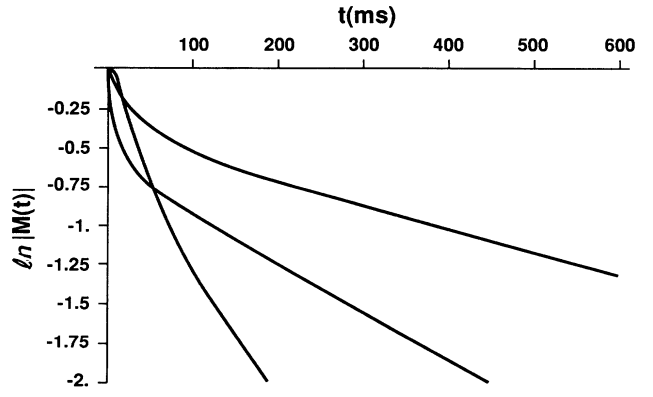

FIG. 18. $\ln|M(t)|$ as a function of t for CPMG envelope for various $t_1=5.1$ and 13.1 ms (from top to bottom). The lowest curve is the second echo envelope for $t=4t_1$. The parameters, which correspond to Bendel's experiment on sand packs, are given in the text.

with the observed crossover time to the linear regime (Fig. 4 of Bendel[14]). Note that $l_c\sim13$ μm, which is about ten times smaller than the pore size R_p. Here we want to make only a qualitative explanation, since the parabolic field is not sufficient to describe the exact local fields, and it would not be meaningful to try to fit more accurately Bendel's curves. However, we would like to emphasize that although the parabolic field is simple, it has the right ingredients which show the crossover to a linear regime. Figure 17 shows the Hahn echo for the parabolic field and corresponds to Fig. 4 of Bendel.[14] Figure 18 shows CPMG with the same pulse spacing t_1 that was employed by Bendel[14] and corresponds to his Fig. 3. By changing the external field one can change g_2 and thus check the predictions of our model, in particular the nonanalytic dependence on g_2.

VI. CONCLUSIONS AND DISCUSSIONS

Our main conclusion is that in porous materials there are intrinsic length scales, associated with the variation of the field gradients, which govern the decay of the magnetization. In this work we have focused our attention on the effect of the curvature of the field, using a simple and solvable model of a parabolic field, but we expect that in more complex fields there will be other length scales. This point has been missed previously, mainly because the approximations widely used in the literature, e.g., the effective uniform gradient or the Gaussian-phase approximation, do not introduce such length scales. For example, the Gaussian-phase approximation for restricted diffusion shows[11] that the linear exponential behavior sets in only for $t\sim R_p^2/D$, and that the magnetization decays as $\exp(-t^3)$ as long as $t\ll R_p^2/D$. This is incorrect when the field has some curvature, e.g., when the gradient is nonuniform, and we find instead that the linear exponential behavior sets in for $t\sim l_c^2/D$, and that l_c can be smaller than R_p. In fact, within the model of artificial pore studied in this paper, the conclusion is that for a single pore the pore size R_p can be effectively replaced by l_c, if $R_p\gg l_c$. This is a strong indication that the curvature of the field plays an important role. If this conclusion holds also for a connected system of pores, it will imply that what is currently thought of as a pore size in porous media should be replaced by the local l_c. We find that at long times the magnetization accumulates in the extremum of the field, and that there the decay is slower than what is generally believed based on constant gradient models of local field. The decay rate is also a nonanalytic function of the curvature g_2, which, again, is a reflection of the breakdown of the Gaussian-phase approximation. Since the internal inhomogeneous field is directly proportional to B_0, the applied field, the former can be varied by varying the latter and can be used to test some of the results in this paper.

A very simplified, but suggestive picture which emerges from the present work, is illustrated in Fig. 1. At very small times the magnetization decays at each point following the $\exp(-D\gamma^2g_1^2t^3/3)$ law in the local uniform gradient $g_1(z)$. At intermediate times it collects around local maxima, minima, and saddle points of the

field, and the echo amplitudes should then be adequately described by the parabolic model studied in this paper, at least if the distances between the hills and valleys of the local field terrain are larger than $l_c=(8D/\gamma g_2)^{1/4}$. At longer times, the diffusion between the regions with minimal gradient becomes important. It is then essential to consider the tunneling between the local extrema of the field, which is implicit in the theory of Ref. 16. By including some microscopic features such as the curvature of the field, the present theory is a very crude attempt to bridge the existing gap between the well-understood very small time limit and the long-time theory of Ref. 16.

The problem of realistic walls will be presented elsewhere.[22] We find that length scales emerge due to the combined effect of wall and inhomogeneity. For instance, in a restricted geometry, such as a slab of size R_p with reflecting boundaries, even a uniform gradient g_1 along the restricted direction gives rise to a natural length scale:

$$l_c^{(1)}=(D/\gamma g_1)^{1/3}$$

and a natural scale $1/T_2=D^{1/3}(\gamma g_1)^{2/3}$ for the decay rate (or bound-states energy). We wish to stress that the above length scale emerges even in the absence of field curvature. Note, unlike the Gaussian-phase approximation, there is a nonanalytic dependence on g_1. The different physical regimes are controlled by the dimensionless parameter $\tilde{g}_1=\gamma g_1 R_p^3/D=(R_p/l_c^{(1)})^3$. For $\tilde{g}_1 \ll 1$ the Gaussian-phase approximation will apply and give a long-time decay rate proportional to $Dg_1^2R_p^4$, as obtained by Robertson[20] and others. However, the validity of this result will be rather limited. As soon as $\tilde{g}_1$ ceases to be very small, the magnetization will become nonuniform and will collect near the boundary (there will be bound states). Thus in general, we expect that T_2 will take the scaling form, analogous to the first term of (5.19):

$$\frac{1}{T_2}=\frac{D}{R_p^2}H[\tilde{g}_1]$$

with $H[v]\sim v^2$ for small v, and $H[v]\sim v^{2/3}$ for large v. This should be true at least for an isolated pore. The exact form of the function $H[v]$ will depend on the details of the geometry, although the asymptotic forms for large and small $\tilde{g}_1$ are related to simple geometric properties of the pore space.[22]

Actually, the wall effects in porous materials are considerably more complicated, because of, for instance, the presence of paramagnetic impurities. The impurities are often modeled by adding to the Torrey[19] equation (2.1) a killing factor at the wall surface as a boundary condition. Note that another interesting consequence of the effects of the curvature of the field is that the killing factor at the boundary might be screened out and considerably reduced if $l_c \ll R_p$ and the magnetization is trapped away from the boundaries (its density close to the wall is reduced).

Finally, it is interesting to note that although the usual motional narrowing arguments are based on the Gaussian-phase approximation, and thus cannot reveal the length scale l_c, it is possible to reconcile *a posteriori*, at least qualitatively, the prediction of the motional narrowing argument with our result. The usual motional narrowing result is

$$1/T_2=1/T_{2B}+\gamma^2\langle H_z^2\rangle_{\rm av}\tau_c \ .$$

Here $\langle H_z^2\rangle_{\rm av}$ is the mean square average of the (random) field seen by the (random walker) spin and τ_c is the correlation time. It is assumed that $\tau_c \ll t \ll T_2$. $\tau_c=L_c^2/D$, where L_c is the correlation length for the random field. According to the argument of Wayne and Cotts[20] spins diffusing in a restricted uniform gradient see a periodic field, and Eq. (6.1) gives the correct result if one takes $L_c=R_p$. Then $\langle g_1^2z^2\rangle_{\rm av}\sim g_1^2R_p^2$ and using $L_c=R_p$, one obtains $1/T_2\sim\gamma^2g_1^2R_p^4/D$, which is the usual second-cumulant result.[19] It turns out that the correct result, i.e., $1/T_2\sim\gamma^2g_2^2l_c^6/D$, i.e., $1/T_2\sim\Omega_0\propto\sqrt{g_2}$ can be obtained from this argument, at least qualitatively, if one uses l_c for all the lengths in the motional narrowing result.

ACKNOWLEDGMENTS

We are grateful to W. Kenyon for discussing his data prior to publication. We are grateful to W. Kenyon, R. Kleinberg, B. I. Halperin, P. Mitra, and A. Sezginer for numerous useful discussions. P.L.D. particularly thanks P. Mitra for very illuminating discussions on the Gaussian-phase approximations, cumulant expansions, and for numerous other comments. P.L.D. thanks M. Oristaglio for making his visit to Schlumberger-Doll Research possible. The Laboratoire de Physique de l'Ecole Normale Superieure is Laboratoire Propre du CNRS Associé à L'ENS et à L'Université Paris–Sud.

APPENDIX: CALCULATION OF SPIN ECHOES

In this appendix the calculation of the successive spin echoes is summarized. This is done using the matrix form for the Green's function as indicated in the text, for the parabolic field with artificially restricted diffusion. We have dropped the subscripts A. We recall that the successive echoes are given by (5.3) and (5.4):

$$\begin{aligned}
M(2t_1)&=\int dz\,dz'\langle z|G(t_1)G(t_1)^*M^*(0)|z'\rangle \ ,\\
M(4t_1)&=\int dz\,dz'\langle z|G(t_1)G(2t_1)^*G(t_1)M(0)|z'\rangle \ ,\\
M(6t_1)&=\int dz\,dz'\langle z|G(t_1)G(2t_1)^*G(2t_1)\\
&\qquad\times G(t_1)^*M(0)^*|z'\rangle \ , \qquad \text{(A1)}
\end{aligned}$$

and so on. An asterisk denotes complex conjugation. First note that $G(2t)=G(t)G(t)$ and thus in the above equations it is clear that the unit which repeats itself is the matrix $S(t_1)=G(t_1)G(t_1)^*G(t_1)^*G(t_1)$, in terms of which one can write

$$M(4nt_1)=\int dz\,dz'\langle z|S(t_1)^nM(0)|z'\rangle \ . \qquad \text{(A2)}$$

The long-time (large-n) behavior and $T_2(t_1)$ are obtained from the lowest eigenvalue of the matrix $S(t_1)$.

The exact calculation is possible because the Green's function is a simple Gaussian function of its arguments [from Eq. (4.3)]:

$$\langle z|G(t_1)|z'\rangle = f\exp[-a(z^2+z'^2)-2bzz'+c(z+z')]\ , \tag{A3}$$

where

$$a=\frac{\Omega}{4D}\coth(\Omega t_1)\ ,\quad b=-\frac{\Omega}{4D\sinh(\Omega t_1)}\ ,$$

$$c=\frac{ig_1\gamma}{\Omega}\tanh\left[\frac{\Omega t_1}{2}\right]=s(a+b)$$

with

$$s=\frac{i4Dg_1\gamma}{\Omega^2}\ ,\quad \Omega^2=-i4Dg_2\gamma+\frac{4}{T_2}\ . \tag{A4}$$

Finally,

$$f=\left[\frac{\Omega}{4\pi D\sinh\Omega t_1}\right]^{1/2} \times\exp\left\{\frac{t_1}{T}-\frac{g_1^2\gamma^2 D}{\Omega^3}\left[\Omega t_1-2\tanh\left[\frac{\Omega t_1}{2}\right]\right]\right\}\ . \tag{A5}$$

Note that $b^2=a^2-(\Omega/4D)^2$. We will also need the following definitions:

$$\alpha=|a|^2+\left[\frac{\Omega}{4D}\right]^2\ ,\quad y=2\left|\frac{\alpha}{b^2}\right|^2-1\ . \tag{A6}$$

Note that when T is finite there is an extra factor $\exp[-(1/2DT)(z^2-z'^2)]$ multiplying the above expression. However, this factor is both real and antisymmetric in z,z'. Thus, when successive matrix Green's functions are multiplied it cancels out and only appears at the edges of the product. Thus we have to keep in mind that for finite T we will have to consider expressions of the form (taking into account the stationary initial distribution)

$$\int dz\,dz'\left[\frac{1}{D\pi T}\right]^{1/2}\exp\left[-\frac{z^2+z'^2}{2DT}\right] \times\langle z|G(t_1)G(t_1)^*\cdots|z'\rangle\ . \tag{A7}$$

For convenience we will thus *not* write explicitly this factor in what follows, but of course it will be taken into account when performing the final spatial integrations.

The first echo is computed from the matrix $R=G(t_1)G^*(t_1)$. One finds that is have a very similar Gaussian form (except for the complex conjugates):

$$\langle z|R|z'\rangle = f_1\exp[-(a_1z^2+a_1^*z'^2)-2b_1zz'+c_1z+c_1^*z'] \tag{A8}$$

with

$$a_1=a-\frac{b^2}{a+a^*}\ ,\quad b_1=-\frac{|b|^2}{a+a^*}\ ,$$

$$c_1=c-b\frac{c+c^*}{a+a^*}\ , \tag{A9}$$

$$f_1=|f|^2\left[\frac{\pi}{a+a^*}\right]^{1/2}\exp\left[\frac{(c+c^*)^2}{4(a+a^*)}\right]\ .$$

Note that f_1 and b_1 are real. From this expression one can obtain a (complicated) expression for the first Hahn echo.

The second echo is computed from the matrix $S(t_1)=G(t_1)G(t_1)^*G(t_1)^*G(t_1)=RR^*$. One finds that again it has a Gaussian form identical to G itself although with different coefficients:

$$\langle z|S(t_1)|z'\rangle = F\exp[-A(z^2+z'^2)-2Bzz'+C(z+z')] \tag{A10}$$

with

$$A=a_1-\frac{b_1^2}{2a_1^*}\ ,\quad B=-\frac{b_1^2}{2a_1^*}\ ,$$

$$C=c_1-b_1\frac{c_1^*}{a_1^*}\ , \tag{A11}$$

$$F=|f_1|^2\left[\frac{\pi}{2a_1^*}\right]^{1/2}\exp\left[\frac{(c_1^*)^2}{2a_1^*}\right]\ ,$$

and, as noted above the even echoes are given by

$$M(4nt_1)=\int dz\,dz'\langle z|S(t_1)^n|z'\rangle\ . \tag{A12}$$

Thus we discover that S itself is a Green's function of yet another quadratic Hamiltonian resembling the one we studied. Since $G=\exp(t_1H)$ where H is the Hamiltonian equal to minus the operator in the rhs of (4.1), we are computing products of the form $\exp(t_1H)\exp(t_1H^*)\cdots$ and since H and H^* do not commute, these are nontrivial. The simplification here is that the Gaussian distribution is stable under convolution, i.e., the resulting operator still has the same Gaussian structure.

1. Determination of $T_2(t_1)$

The matrix S has $\phi(z)=\exp(-rz^2-pz)$ as its ground state and eigenvalue λ with

$$r=(A^2-B^2)^{1/2}\ ,\quad p=C\frac{A-B+(A^2-B^2)^{1/2}}{A+B+(A^2-B^2)^{1/2}}\ ,$$

$$\lambda=f\left[\frac{\pi}{A+(A^2-B^2)^{1/2}}\right]^{1/2} \times\exp\left[C^2\frac{A+(A^2-B^2)^{1/2}}{[A+B+(A^2-B^2)^{1/2}]^2}\right]\ . \tag{A13}$$

Thus one has, for large n,

$$M(4nt_1)\sim\exp[-\ln(\lambda)n]=\exp\left[-\frac{\ln(\lambda)}{4t_1}t\right]\ . \tag{A14}$$

Note that this is very similar to (5.9) and (5.10) and that $\phi(z)$ is similar to $\psi_0(z)$ in (5.10). Thus for fixed t_1 when $t \to \infty$ there is also a characteristic size $l_c(t_1)$ of the packet of magnetization in the CPMG experiment. For $R_p = \infty$ it is given by

$$l_c(t_1) = [\mathrm{Re}(r)]^{-1/2} , \tag{A15}$$

where r is given in (A13).

Using (A9)–(A14) we finally arrive at the following result for $T_2(t_1)$ as the sum of two decay rates:

$$1/T_2(t_1) = 1/T^{(1)} + 1/T^{(2)} . \tag{A16}$$

$T^{(1)}$ depends only on g_2 and T (and not on g_1). It vanishes for any T when $g_2 = 0$ as expected since then there is no decay. It is the only piece which remains when $g_1 = 0$ (or for $T = \infty$ for any g_1):

$$\frac{1}{T^{(1)}} = \frac{1}{8t_1} \ln[y + (y^2-1)^{1/2}] - \frac{1}{T} , \tag{A17}$$

where y is given by (A4) and (A6).

The second piece $T^{(2)}$ is proportional to Dg_1^2 and vanishes when $g_2 = 0$. When $T = \infty$ and $g_2 > 0$ it does not depend on g_1 (because in that case the second term cancels exactly the term proportional to tanh in the first). One finds

$$\frac{1}{T^{(2)}} = \mathrm{Re}\left[\frac{\gamma^2 g_1^2 D}{\Omega^3 t_1} [\Omega t_1 - 2\tanh(\Omega t_1/2)] \right] + \frac{-1}{4t_1(a+a^*)} \left[2\{\mathrm{Re}[(a+b)s]\}^2 + \mathrm{Re}(s^2\alpha) - |sb|^2 - 4\mathrm{Im}(s)\mathrm{Im}(sa^*b) - 4(\mathrm{Im}s)^2 \frac{\mathrm{Re}(a^2 b^{*2}\alpha) - |a|^2|b|^4}{|\alpha|^2 - |b|^4} \right] . \tag{A18}$$

It is interesting to compare this result for the decay of the CPMG echoes to the decay of the local magnetization of Sec. IV (FID), which is easily obtained from the Green's function (A3) and (A4):

$$M(z,t) = \left[\frac{1}{\pi D T \cosh\Omega t} \right]^{1/2} \exp\left[\frac{-\gamma^2 g_1^2 D}{\Omega^3} (\Omega t - \tanh\Omega t) + i \left[\frac{\tanh\Omega t}{\Omega} \right] \gamma g_1 z \right] \exp\left[-\frac{z^2}{4D} \left[\frac{2}{T} + \Omega \tanh(\Omega t) \right] \right] . \tag{A19}$$

When $g_2 = 0$, $T^{(2)}$ simplifies and becomes equal to

$$\frac{1}{T^{(2)}} = \frac{\gamma^2 g_1^2 D}{\Omega^3 t_1} (\Omega t_1 - \tanh\Omega t_1) , \tag{A20}$$

where now $\Omega = 2/T$. Thus, in this particular case we find that it is identical to the decay of the local magnetization (A19), e.g., the product rule for the decay is correct. It fails, however, as soon as $g_2 > 0$. Since $g_2 = 0$ is precisely the case where the phase distribution is exactly Gaussian (see Sec. IV) we conclude that the product rule is wrong precisely when the phases are not Gaussian.

For large t_1 it is possible to obtain the decay for the CPMG sequence quite nicely using the property of ground-state dominance. We give the derivation here because it can in principle be used to study other field profiles dominated by a ground state. Using (5.9) one gets for large t_1

$$M(t = 2nt_1) = \left| \int dz \frac{1}{(\pi DT)^{1/4}} e^{-z^2/2DT} \psi_0(z) \right|^2 \left[\int dz |\psi_0(z)|^2 \right]^n \exp[-\mathrm{Re}(E_0)t] , \tag{A21a}$$

where for even echoes (n even) the absolute value squared in the first term is replaced by a simple square. There is thus an even-odd effect. Thus we find the following general expression for large t_1:

$$\frac{1}{T_2(t_1)} = \frac{1}{T_{2D}} - \frac{1}{2t_1} \ln\left[\int dz |\psi_0(z)|^2 \right] + \text{h.o.t} , \tag{A21b}$$

where the higher-order terms (h.o.t.) are *exponentially* decaying functions of t_1 (if the spectrum is discrete). In particular, for $g_1 = 0$ we find simply

$$\frac{1}{T_2(t_1)} = \frac{1}{T_{2D}} - \frac{1}{4t_1} \ln\left[\frac{|\Omega|}{\mathrm{Re}(\Omega)} \right] + \text{h.o.t.} \tag{A22}$$

2. Determination of M ($t = 4nt_1$) as a function of t

In the last subsection we obtained the asymptotic decay rate for a large number of echoes. In fact it is also possible to obtain an exact expression for an arbitrary n.

For simplicity we choose here $g_1=0$. We observed that $S(t_1)$ has a form very similar to $G(t_1)$. In fact, defining

$$A=r\coth(\Phi)\ ,\quad B=-r/\sinh(\Phi)$$

or equivalently,

$$r=(A^2-B^2)^{1/2}\ ,\quad \Phi=\ln(A+r)-\ln B\ , \tag{A23}$$

one sees from the convolution rules of the Gaussian that $S(t_1)^n$ has the same form as $S(t_1)$ with A,B replaced by

$$A_n=r\coth(n\Phi)\ ,\quad B_n=-r/\sinh(n\Phi) \tag{A24}$$

(which is precisely why the harmonic oscillator Green's function is solvable). Thus it is now simple, copying the result (4.8) (with $k=0$) to obtain

$$M(t=4nt_1)=\left[\frac{4rDT}{[1+2rDT\coth(n\Phi/2)][1+2rDT\tanh(n\Phi/2)]\sinh n\Phi}\right]^{1/2}e^{t/T}\ , \tag{A25}$$

which was used to plot Figs. 15 and 16. Replacing in the above expression n by $t/(4t_1)$, we find that $\ln[|M(t)|]$ starts linearly for small t with a slope

$$\frac{1}{T_2(t_1)}+\frac{\Phi}{8t_1}\left[\mathrm{Tr}+\frac{1}{4Tr}-1\right]\ . \tag{A26}$$

*On leave from Laboratoire de Physique de l' Ecole Normale Superieure, 24 rue Lhomond, Paris 75231 CEDEX 05, France.

[1]R. M. Cotts, Nature (London) **351**, 467 (1991).

[2]W. Kenyon, J. Howard, A. Sezginer, C. Straley, A. Matteson, K. Horkowitz, and R. E. Ehrlich (unpublished); K. R. Brownstein and C. E. Tarr, Phys. Rev. A **19**, 2446 (1979); D. O. Seevers (unpublished); C. H. Neuman and R. J. S. Brown, J. Pet. Technol. 2853-62 (1982); A. Timur, *ibid.* **21**, 775 (1969); R. J. S. Brown, Nature (London) **189**, 388 (1961); J. D. Robinson and J. D. Loren, Soc. Pet. Eng. J. **249**, 268 (1970).

[3]R. L. Kleinberg and M. A. Horsfield, J. Magn. Reson. **88**, 9 (1990), and references therein.

[4]F. D'Orazio, S. Bhattacharja, W. P. Halperin, and R. Gerhardt, Phys. Rev. **42**, 6503 (1990), and references therein.

[5]E. O. Stejskal, J. Chem. Phys. **43**, 3597 (1965).

[6]P. T. Callaghan, Aust. J. Phys. **37**, 359 (1984).

[7]M. Lipsicas, J. R. Banavar, and J. Willemesen, App. Phys. Lett. **48**, 1544 (1986).

[8]P. T. Callaghan, D. MacGowan, K. J. Packer, and F. O. Zeleya, Nature (London) **351**, 467 (1991); J. Magn. Reson. **90**, 177 (1990).

[9]W. P. Rothwell and H. J. Vinegar, App. Opt. **24**, 3969 (1985); H. J. Vinegar, P. N. Tutunjian, P. T. Crabtree, F. J. Raffald, R. DiJoggio,and W. A. Edelstein, Log Anal. **32**, 527 (1991); D. E. Woessner, J. W. Gleeson, and C. F. Jordan, in Proceedings of 65th Annual Society of Petroleum Engineering Conference, 1990 (Soc. Pet. Eng., Houston, to be published); C. Chardaire-Riviere and J-C Roussel, in Proc. 5th Annual Soc. Core Analysts, 1991 (Soc. Core Analysts, Houston, to be published); P. Bendel, IEE Trans. Med. Imaging **MI-4**, 114 (1985).

[10]R. F. Karlicek, Jr. and I. J. Lowe, J. Magn. Reson. **37**, 75 (1980); R. M. Cotts, M. J. R. Hoch, T. Sun, and J. T. Marker, *ibid.* **83**, 252 (1989).

[11]J. C. Tarczon and W. P. Halperin, Phys. Rev. B **32**, 2798 (1985).

[12]J. A. Glasel and K. H. Lee, J. Am. Chem Soc. **96**, 970 (1974).

[13]S. Majumdar and J. C. Gore, J. Magn. Reson. **78**, 41 (1988).

[14]P. Bendel, J. Magn. Reson. **86**, 509 (1990).

[15]R. L. Kleinberg, A. Sezginer, D. D. Griffin, and M. Fukuhara (unpublished).

[16]P. P. Mitra and P. Le Doussal, Phys. Rev. B **44**, 12035 (1991); P. P. Mitra, P. Le Doussal, and B. I. Halperin (unpublished); P. Le Doussal (unpublished).

[17]W. E. Kenyon (unpublished).

[18]E. L. Hahn, Phys. Rev. **80**, 580 (1950); H. Y. Carr and E. M. Purcell, *ibid.* **94**, 630 (1954); T. P. Das and A. K. Saha, *ibid.* **93**, 749 (1954); S. Meiboom and D. Gill, Rev. Sci. Instrum. **29**, 688 (1958).

[19]H. C. Torrey, Phys. Rev. **104**, 563 (1956).

[20]R. C. Wayne and R. M. Cotts, Phys. Rev. **151**, 264 (1966); B. Robertson, *ibid.* **151**, 273 (1966); C. H. Neumann, J. Chem. Phys. **60**, 4508 (1974); J. S. Murday and R. M. Cotts, *ibid.* **48**, 4938 (1968).

[21]P. P. Mitra and P. N. Sen, Phys. Rev. B **45**, 143 (1992).

[22]P. Le Doussal, P. Mitra, and P. N. Sen (unpublished).

[23]M. Kac, Am. Math Month **54**, 369 (1947), reprinted in *Noise and Stochastic Processes,* edited by N. Wax (Dover, New York 1954).

[24]R. P. Feynman, *Statistical Mechanics* (Addison-Wesley, New York, 1972).

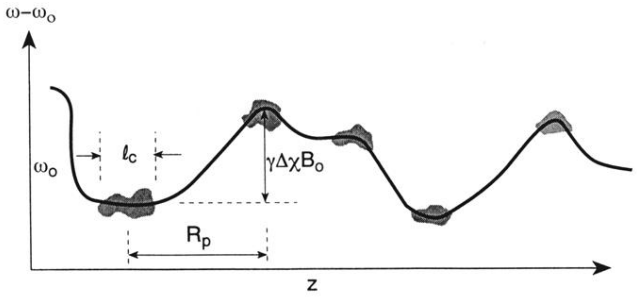

FIG. 1. A schematic diagram showing a possible terrain of local magnetic field, in a pore of a random medium, as a function of distance. Dots are to show the accumulation of magnetization at the extrema.